

Proposal to JLab PAC 53

Double Deeply Virtual Compton Scattering
with SoLID μ spectrometer

Zhiwen Zhao

SoLID Collaboration Meeting
June 7-8, 2025

Proposal to PAC53 PR12-25-010

Proposal to JLab PAC 53

Double Deeply Virtual Compton Scattering with SoLID μ spectrometer

Xinzhan Bai*, Alexandre Camsonne†, Silviu Covrig Dusa, Kondo Gnanvo, Dave Mack, Michael McCaughan, and Richard Tyson

Thomas Jefferson National Accelerator Facility, Newport News, VA, USA

Juan-Sebastian Alvarado*, Raphaël Dupré, Adam Hobart, Dominique Marchand, Carlos Muñoz Camacho, Silvia Niccolai, and Eric Voutier*

Université Paris-Saclay, CNRS/IN2P3/IJCLab, Orsay, France

Haiyan Gao, Yining Liu, Bo Yu, Yi Yu, Zhiwen Zhao*, and Jingyi Zhou

Duke University, Durham, NC, USA

Keagan Bell, Debaditya Biswas, Marie Boër*, Gyang Chung, Mahmoud Gomina, Arna Ma, and Kemal Tezgin

Virginia Tech, Blacksburg, VA, USA

Garth Huber, Nathan Heinrich, Muhammad Junaid, Vijay Kumar, and Alicia Postuma

University of Regina, Regina, SK, Canada

Ronald Gilman

Rutgers University, Piscataway, NJ, USA

Nilanga Linayage, Huong Thi Nguyen, and Asar Ahmed

University of Virginia, Charlottesville, VA, USA

Yi Wang, Junhuai Xu, Zhihong Ye, Haojie Zhang, and Yaopeng Zhang

Tsinghua University, Beijing, China

Evaristo Cisbani

Istituto Superiore di Sanità, Roma, Italia

Guido Maria Urcioli

INFN, Sezione di Roma1, Roma, Italia

Vincenzo Bellini and Concetta Maria Sutura

Università di Catania, Catania, Italia

Anthony W. Thomas

*ARC Special Research Centre for the Subatomic Structure of Matter (CSSM),
University of Adelaide, Adelaide, Australia*

Pierre Chatagnon¹, Maxime Defurne¹, Víctor Martínez-Fernández^{1,2}, Hervé Moutarde¹, and Franck Sabatié¹

¹ *IRFU, CEA, Université Paris-Saclay, Gif-sur-Yvette, France*

² *Center for Frontiers in Nuclear Science, Stony Brook University, Stony Brook, NY, USA*

Malek Mazouz and Wassim Hamdi

Faculté des Sciences de Monastir, Département de Physique, Monastir, Tunisia

Whitney Armstrong, Sylvester Joosten, and Zein-Eddine Meziani

Argonne National Laboratory, Physics Division, Argonne, IL, USA

Thomas Hemmick

Stony Brook University, Stony Brook, NY, USA

Bernard Pire

Centre de Physique Théorique, CNRS, École polytechnique, I.P. Paris, Palaiseau, France

Pawel Sznajder and Jakub Wagner

National Centre for Nuclear Research, NCBJ, Warsaw, Poland

Johan A. Colorado-Caicedo

Centro de Investigacion y de Estudios Avanzados del Instituto Politecnico Nacional, San Pedro Zacatenco, Mexico City, Mexico

Sudip Bhattacharya

Idaho State University, Pocatello, ID, USA

Nikos Sparveris, Hamza Atac, Suman Shrestha, and Mazmus. Ifat

Temple University, Philadelphia, PA, USA

Mostafa Elaasar

Southern University at New Orleans, New Orleans, LA, USA

Darko Androić

University of Zagreb, Faculty of Science, Zagreb, Croatia

Eric Fuchey

College of William & Mary, Williamsburg, Virginia, USA

Hem Bhatt

Mississippi State University, Mississippi State, MS, USA

Pawel Nadel-Turonski

University of South Carolina, Columbia, SC, USA

Xiaqing Li, Tianbo Liu, and Weizhi Xiong

Shandong University, Qingdao, Shandong, China

*: Co-spokesperson, †: Contact-spokesperson (camsonne@jlab.org)

And SoLID Collaboration

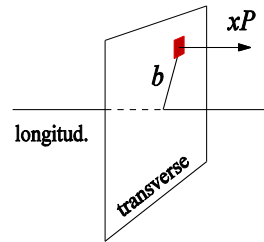
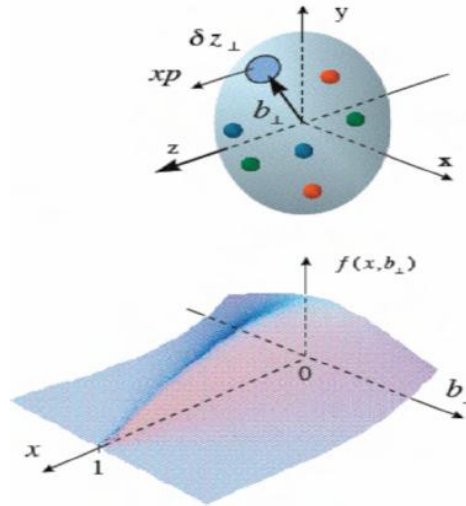
Spokesperson : Juan-Sebastian Alvarado, Alexandre Camsonne, Marie Boer,
Eric Voutier, Xinzhan Bai, Zhiwen Zhao

Overview

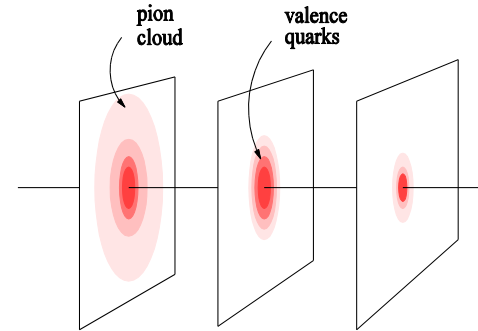
- General Parton Distribution
- Double Deeply Virtual Compton Scattering
- SoLID μ setup
- Muon detector
- Simulation study
- Physics projections
- Beam time request
- Summary

Generalized Parton Distribution (GPD)

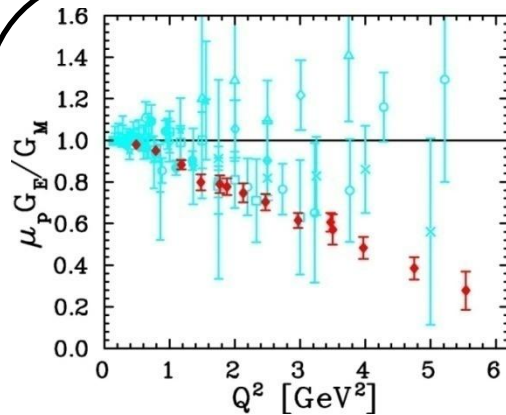
A unified descriptions of partons (quarks and gluons) in the momentum and impact parameter space



(a)

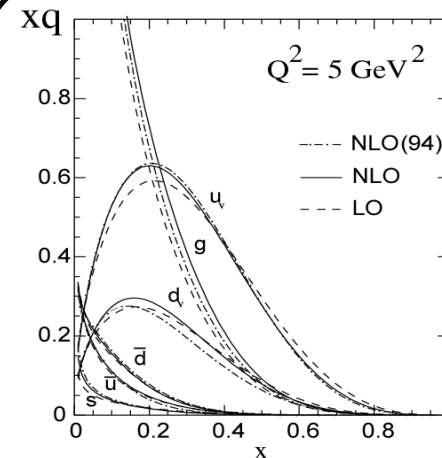
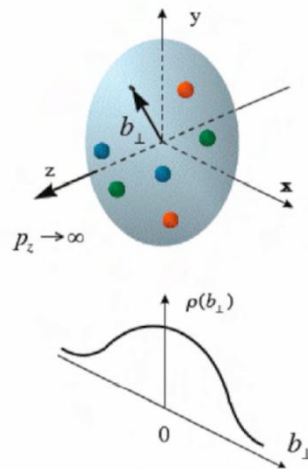


(b) $x < 0.1$ $x \sim 0.3$ $x \sim 0.8$



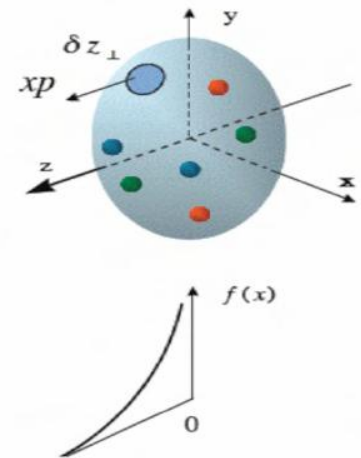
Elastic form factors

Transverse spatial distributions



Parton Distribution Functions

Longitudinal momentum distributions



General Compton Process accessing GPD

$$\gamma^*(q) + p(p) \rightarrow \gamma^*(q') + p(p')$$

$$Q^2 = -q^2, \quad Q'^2 = q'^2, \quad s = (p + q)^2, \quad t = \Delta^2,$$

Deeply Virtual CS ($\gamma' \rightarrow \gamma, Q'^2=0, \xi' = \xi$)
 Timelike CS ($\gamma \rightarrow \gamma', Q^2=0, \xi' = -\xi$)
 Double DVCS ($\gamma' \rightarrow \gamma'$)

Because of the virtuality of the final photon, **DDVCS** allows a direct access to GPDs at $x \neq \pm\xi$, which is of importance for their modeling and for the investigation of **nuclear dynamics**.

Compton Form Factor (CFF)

$$\mathcal{F}(\xi', \xi, t) = \mathcal{P} \int_{-1}^1 F_+(x, \xi, t) \left[\frac{1}{x - \xi'} \pm \frac{1}{x + \xi'} \right] dx - i\pi F_+(\xi', \xi, t)$$

GPD combination

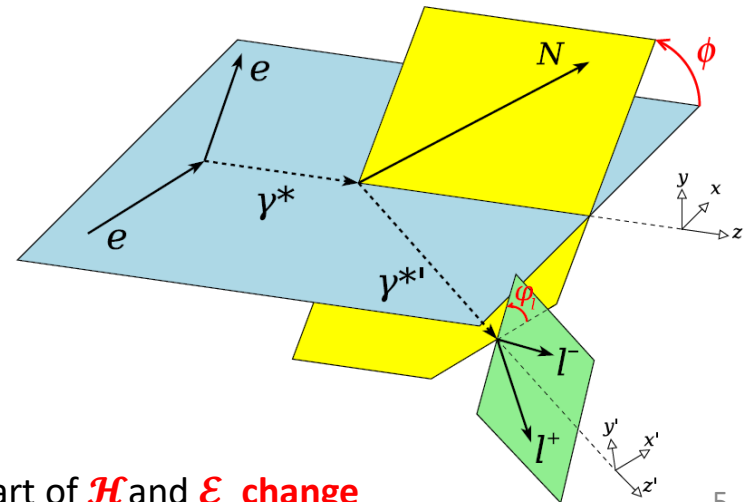
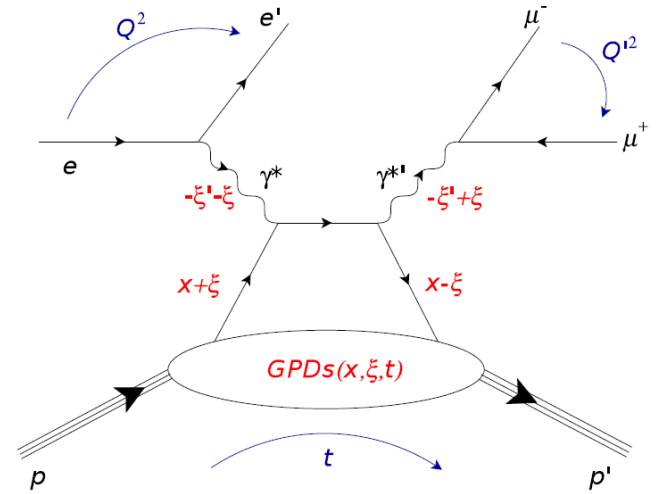
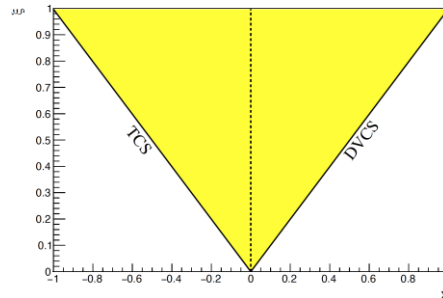
$$F_+(x, \xi, t) = \sum_q \left(\frac{e_q}{e} \right)^2 [F^q(x, \xi, t) \mp F^q(-x, \xi, t)]$$

Generalized Bjorken variable

$$\xi' = \frac{Q^2 - Q'^2 + t/2}{2Q^2/x_B - Q^2 - Q'^2 + t}$$

Skewness

$$\xi = \frac{Q^2 + Q'^2}{2Q^2/x_B - Q^2 - Q'^2 + t}$$

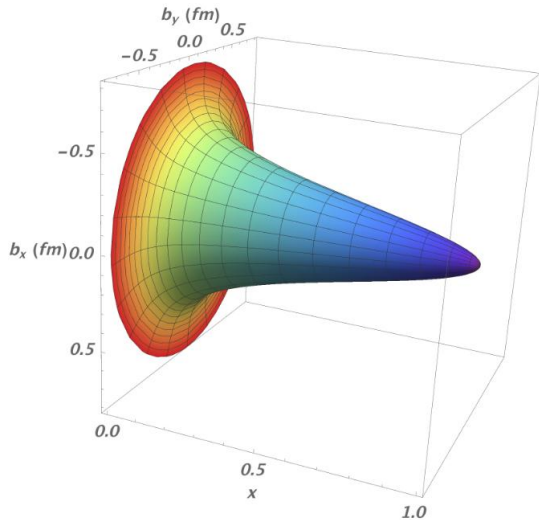


Following the sign change of ξ around $Q'^2=Q^2$, the imaginary part of \mathcal{H} and \mathcal{E} change sign, providing a testing ground of **GPD universality**.

Nucleon Femtography

M. Burkardt PRD 62 (2000) 071503. M. Diehl EPJC 25 (2002) 223 A.V. Belitsky, D. Müller, NPA 711 (2002) 118c J.P. Ralston; B. Pire PRD 66 (2002) 111501

$$\rho_H^q(x, \mathbf{b}_\perp) = \int \frac{d^2 \Delta_\perp}{(2\pi)^2} e^{i\mathbf{b}_\perp \cdot \Delta_\perp} [H^q(x, 0, -\Delta_\perp^2) + H^q(-x, 0, -\Delta_\perp^2)]$$



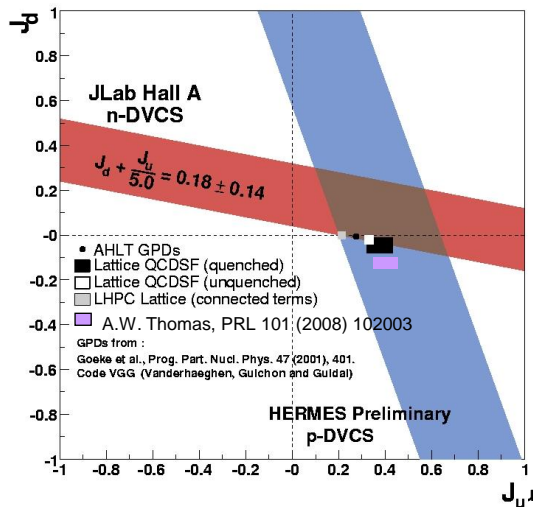
- The **transverse densities** of partons in nucleons and nuclei is related to the transverse momentum transfer ($-\Delta_\perp^2$) dependence of GPDs at **zero-skewness**.
- **DVCS** and **TCS** cannot map out **zero-skewness GPDs** over the **full physics phase space**.

The **experimental knowledge** of the **ξ -dependence** of GPDs at fixed longitudinal momentum fraction allows to **control** the **zero-skewness extrapolation** required for **nucleon imaging**.

R. Dupré, M. Guidal, M. Vanderhaeghen, PRD 95 (2017) 011501

Nucleon Spin

$$\lim_{t \rightarrow 0} \int_{-1}^1 x [H^q(x, \xi, t) + E^q(x, \xi, t)] dx = J^q$$

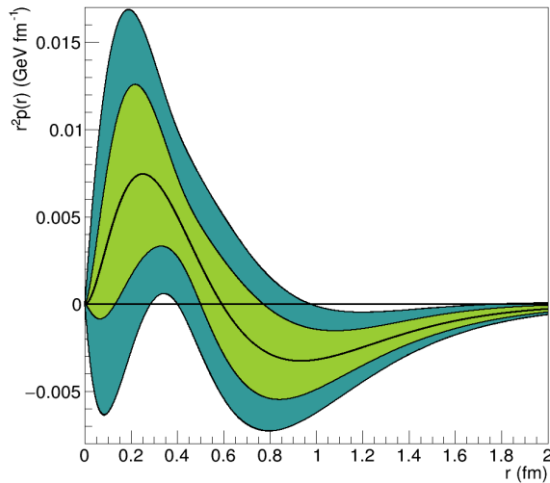


- The **total angular momentum of partons** inside the nucleon can be inferred from the Ji sum rule which involves the **forward limit** of the **first Mellin moment** of partons helicity conserving GPDs.
- **DVCS** and **TCS** cannot access GPDs at $x \neq \xi$ over the **full physics phase space**.

The **experimental knowledge** of the **ξ -dependence** of GPDs at fixed longitudinal momentum fraction is a **mandatory step** for unraveling the **nucleon spin**.

Nucleon Forces

$$\int_{-1}^1 x \sum_q H^q(x, \xi, t) dx = M_2(t) + \frac{4}{5} \xi^2 d_1(t)$$



- The **skewness dependence** of the **first Mellin moment** of the GPD H provides an access to the **gravitational form factors** of the energy momentum tensor of the nucleon.
- **e^\pm -DVCS** and **TCS** offers another path via **dispersion relations**.

The **ξ -dependence** of GPDs reveals the **internal dynamics** of the nucleon.

V. Burkert, L. Elouadrhiri, F.-X. Girod, Nat. 557 (2018) 396; arXiv:2104.02031

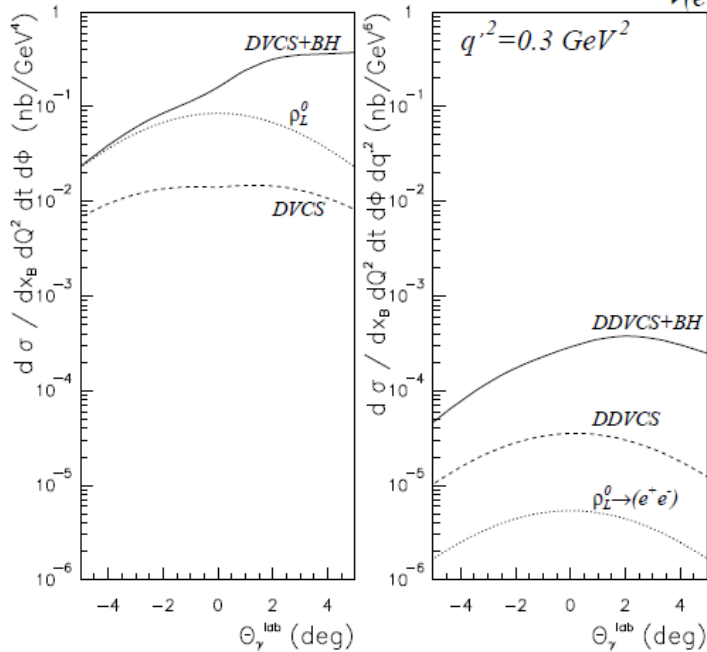
Elementary Cross Section

DDVCS cross section is about **1/100** of **DVCS** and involves two Bethe-Heitler

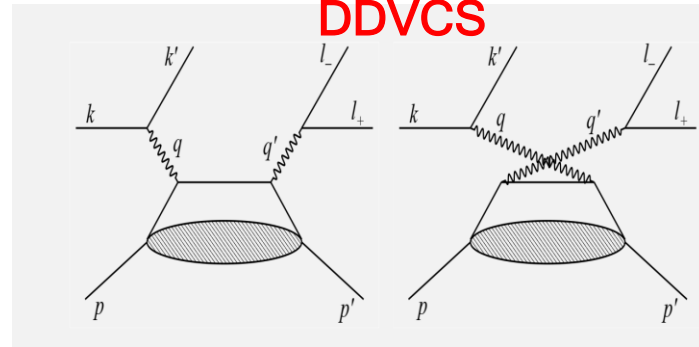
$$d^7\sigma_P^e = d^7\sigma_{BH_1} + d^7\sigma_{BH_2} + d^7\sigma_{DDVCS} + P d^7\tilde{\sigma}_{DDVCS} + d^7\sigma_{INT_2} + P d^7\tilde{\sigma}_{INT_2} - e [d^7\sigma_{BH_{12}} + d^7\sigma_{INT_1} + P d^7\tilde{\sigma}_{INT_1}]$$

$$E_e = 6 \text{ GeV}, Q^2 = 2.5 \text{ GeV}^2, x_B = 0.3, \Phi = 0 \text{ deg.}$$

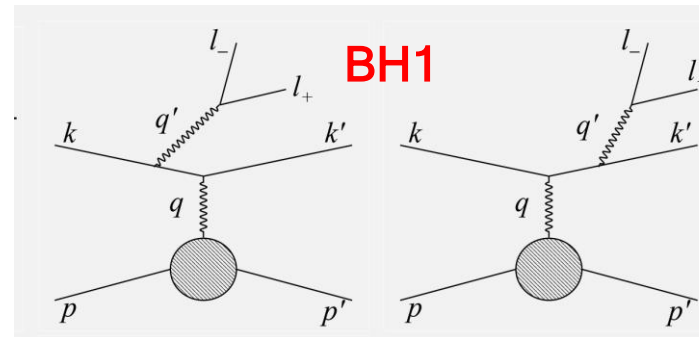
$$e^- + p \rightarrow e^- + p + \gamma, \rho_L^0 \quad e^- + p \rightarrow e^- + p + (\gamma, \rho_L^0) \rightarrow (e^- e^+)$$



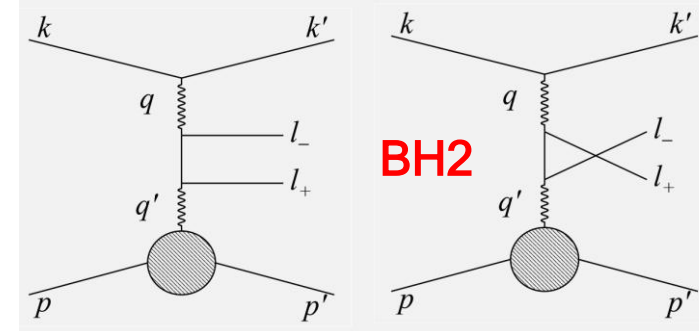
DDVCS



BH1



BH2



Integrated Cross Section

5-fold observables obtained from the **integration over** the **polar angle** of the **muon** and the **azimuthal angle** of the **final virtual photon** or the **initial virtual photon** are required, also **minimizing** the contribution of the **BH₂** process.

DVCS-like

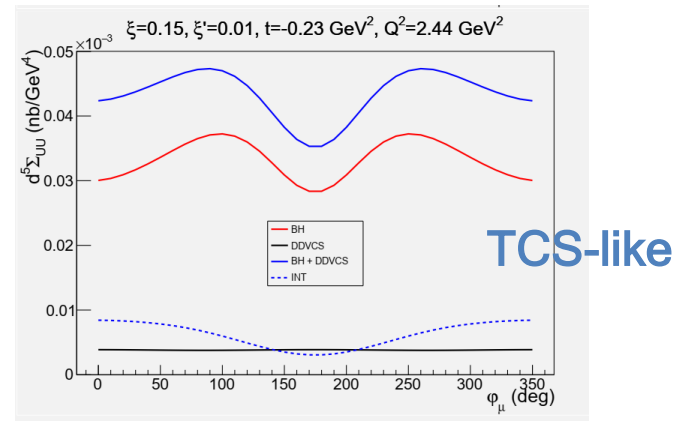
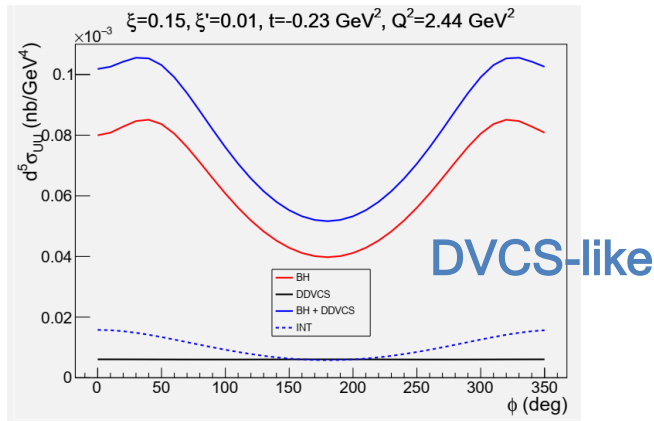
$$d^5\sigma^\lambda(\phi) \equiv \frac{d^5\sigma^\lambda(\phi)}{dx_B dy dt dQ'^2 d\phi} = \int_0^{2\pi} d\varphi_\mu \int_{\pi/2-\theta_0}^{\pi/2+\theta_0} d\theta_\mu \sin(\theta_\mu) \frac{d^7\sigma^\lambda(\phi, \theta_\mu, \phi_\mu)}{dx_B dy dt d\phi dQ'^2 d\Omega_\mu}$$

$$d^5\sigma^\lambda = d^5\sigma_{BH_1} + d^5\sigma_{BH_2} + d^5\sigma_{DDVCS} + d^5\sigma_{\mathcal{I}_1} + \lambda d^5\tilde{\sigma}_{\mathcal{I}_1} = d^5\sigma_{UU} + \lambda d^5\sigma_{LU}$$

TCS-like

$$d^5\Sigma^\lambda(\varphi_\mu) \equiv \frac{d^5\sigma^\lambda(\varphi_\mu)}{dx_B dy dt dQ'^2 d\varphi_\mu} = \int_0^{2\pi} d\phi \int_{\pi/2-\theta_0}^{\pi/2+\theta_0} d\theta_\mu \sin(\theta_\mu) \frac{d^7\sigma^\lambda(\phi, \theta_\mu, \phi_\mu)}{dx_B dy dt d\phi dQ'^2 d\Omega_\mu}$$

$$d^5\Sigma^\lambda = d^5\Sigma_{BH_1} + d^5\Sigma_{BH_2} + d^5\Sigma_{BH_{12}} + d^5\Sigma_{DDVCS} + d^5\Sigma_{\mathcal{I}_1} + d^5\Sigma_{\mathcal{I}_2} + \lambda d^5\tilde{\Sigma}_{\mathcal{I}_2} = d^5\Sigma_{UU} + \lambda d^5\Sigma_{LU}$$

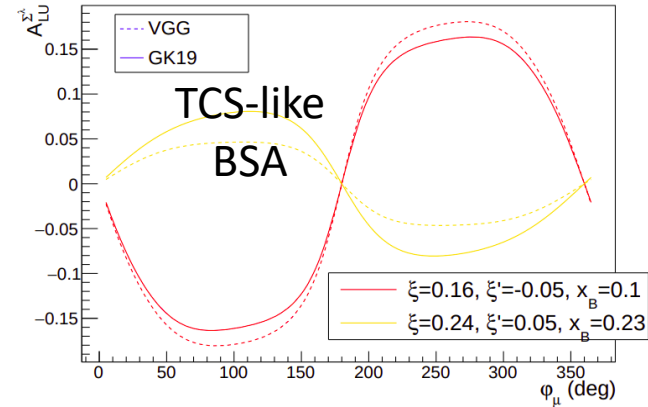
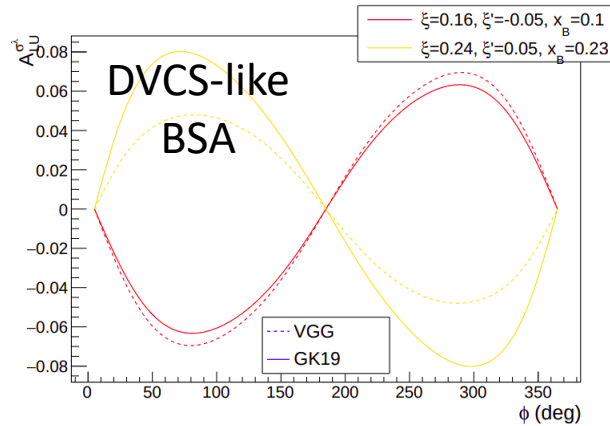


Beam Spin Asymmetry

$$A_{LU}^{\sigma^\lambda} \equiv A_{LU}^{\sigma^\lambda}(\phi) = \lambda \frac{d^5\sigma^+ - d^5\sigma^-}{d^5\sigma^+ + d^5\sigma^-} = \frac{\lambda d^5\tilde{\sigma}_{\mathcal{I}_1}}{d^5\sigma_{BH_1} + d^5\sigma_{BH_2} + d^5\sigma_{DDVCS} + d^5\sigma_{\mathcal{I}_1}} \quad (29)$$

$$A_{LU}^{\Sigma^\lambda} \equiv A_{LU}^{\Sigma^\lambda}(\varphi_\mu) = \lambda \frac{d^5\Sigma^+ - d^5\Sigma^-}{d^5\Sigma^+ + d^5\Sigma^-} = \frac{\lambda d^5\tilde{\Sigma}_{\mathcal{I}_2}}{d^5\Sigma_{BH_1} + d^5\Sigma_{BH_2} + d^5\Sigma_{BH_{12}} + d^5\Sigma_{DDVCS} + d^5\Sigma_{\mathcal{I}_1} + d^5\Sigma_{\mathcal{I}_2}} \quad (30)$$

$$A_{LU}^{S^\lambda} \propto \Im \left\{ F_1 \mathcal{H} + \xi' (F_1 + F_2) \tilde{\mathcal{H}} - \frac{t}{4M_N^2} F_2 \mathcal{E} \right\}$$



- Access to the imaginary part of CFFs
- Sign change when transitioning from DVCS region ($\xi' > 0, Q^2 > Q'^2$) to TCS region ($\xi' < 0, Q^2 < Q'^2$)
- **TCS(DVCS)**-like BSA enhances the amplitude in the $\xi' < 0$ ($\xi' > 0$) region
- **DDVCS BSAs** are **dominated** by the CFF **H** as DVCS and TCS, thus providing a similar quality measurement of the **H** GPD at $\xi' \neq \pm \xi$

Muon Charge Asymmetry

$$A_{UU}^{FB}(\varphi_\mu) = \frac{d^5\Sigma_{UU}(\varphi_{\mu-}) - d^5\Sigma_{UU}(\varphi_{\mu-} + \pi)}{d^5\Sigma_{UU}(\varphi_{\mu-}) + d^5\Sigma_{UU}(\varphi_{\mu-} + \pi)} = \frac{d^5\Sigma_{UU}(\varphi_{\mu-}) - d^5\Sigma_{UU}(\varphi_{\mu+})}{d^5\Sigma_{UU}(\varphi_{\mu-}) + d^5\Sigma_{UU}(\varphi_{\mu+})} = A_{UU}^{\mu\pm}(\varphi_\mu)$$

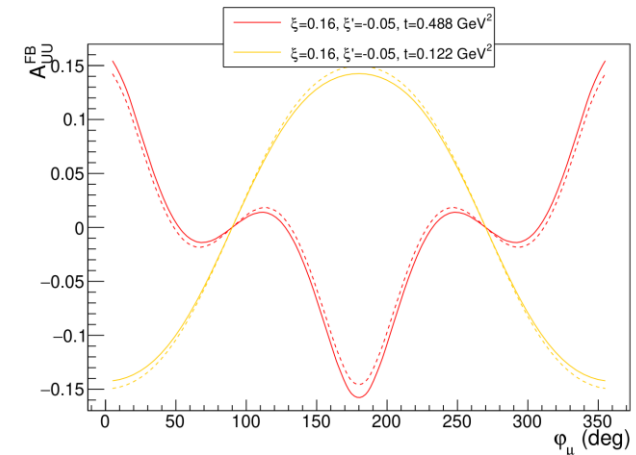
$$d^5\Sigma_{UU}(\varphi_{\mu-} + \pi) = \int_0^{2\pi} d\phi \int_{\pi/2-\theta_0}^{\pi/2+\theta_0} d\theta_{\mu-} \sin(\theta_{\mu-}) \frac{d^7\sigma^0(\phi, \pi - \theta_{\mu-}, \varphi_{\mu-} + \pi)}{dx_B dy dt d\phi dQ'^2 d\Omega_{\mu-}}$$

$$= \int_0^{2\pi} d\phi \int_{\pi/2-\theta_0}^{\pi/2+\theta_0} d\theta_{\mu+} \sin(\theta_{\mu+}) \frac{d^7\sigma^0(\phi, \theta_{\mu+}, \varphi_{\mu+})}{dx_B dy dt d\phi dQ'^2 d\Omega_{\mu+}} = d^5\Sigma_{UU}(\varphi_{\mu+})$$

aka Forward Backward Asymmetry

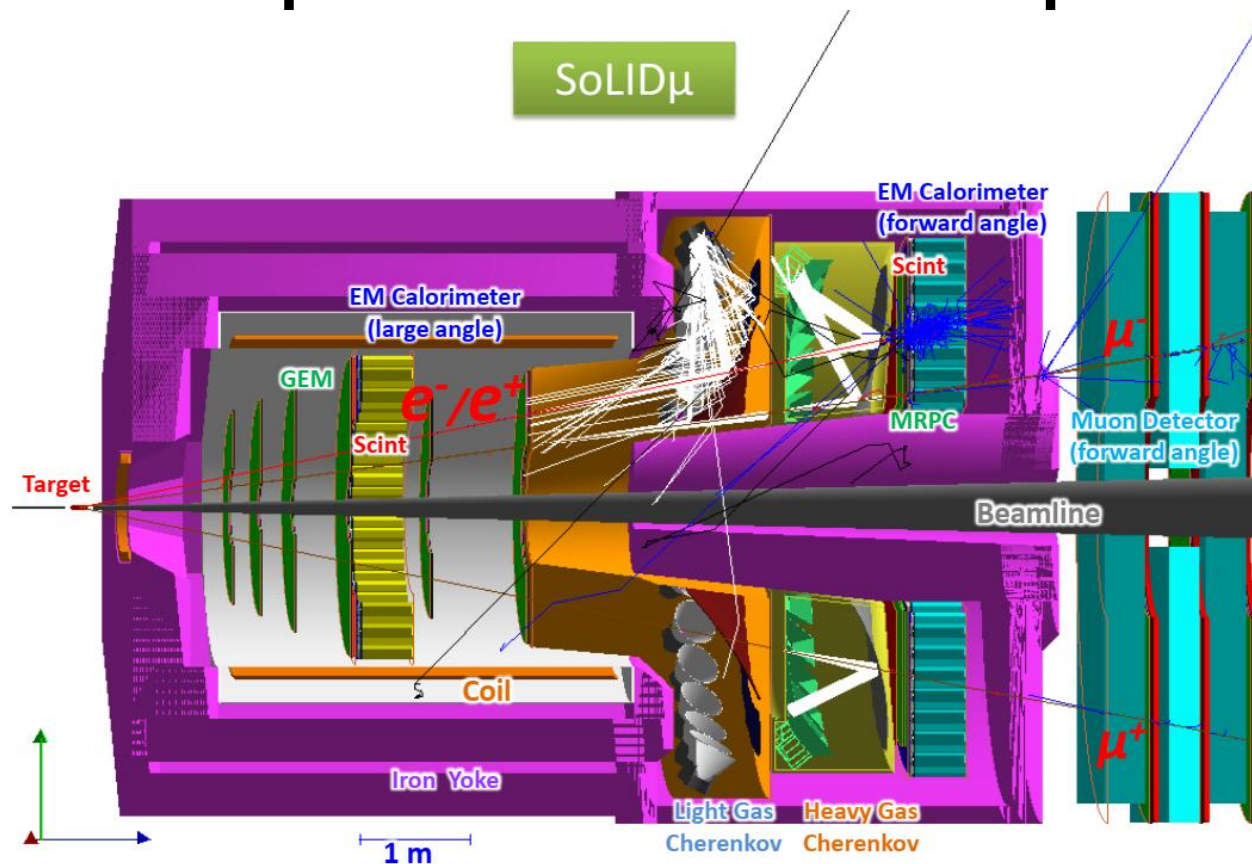
$$A_{UU}^{\mu\pm}(\varphi_\mu) = \frac{d^5\Sigma_{BH_{12}} + d^5\Sigma_{\mathcal{I}_2}}{d^5\Sigma_{BH_1} + d^5\Sigma_{BH_2} + d^5\Sigma_{DDVCS} + d^5\Sigma_{\mathcal{I}_1}}$$

$$d^5\Sigma_{\mathcal{I}_2} \propto -\frac{\xi'}{\xi} \Re \left[F_1 \mathcal{H} + \frac{\xi^2}{\xi'} (F_1 + F_2) \tilde{\mathcal{H}} - \frac{t}{4M_N^2} F_2 \mathcal{E} \right]$$



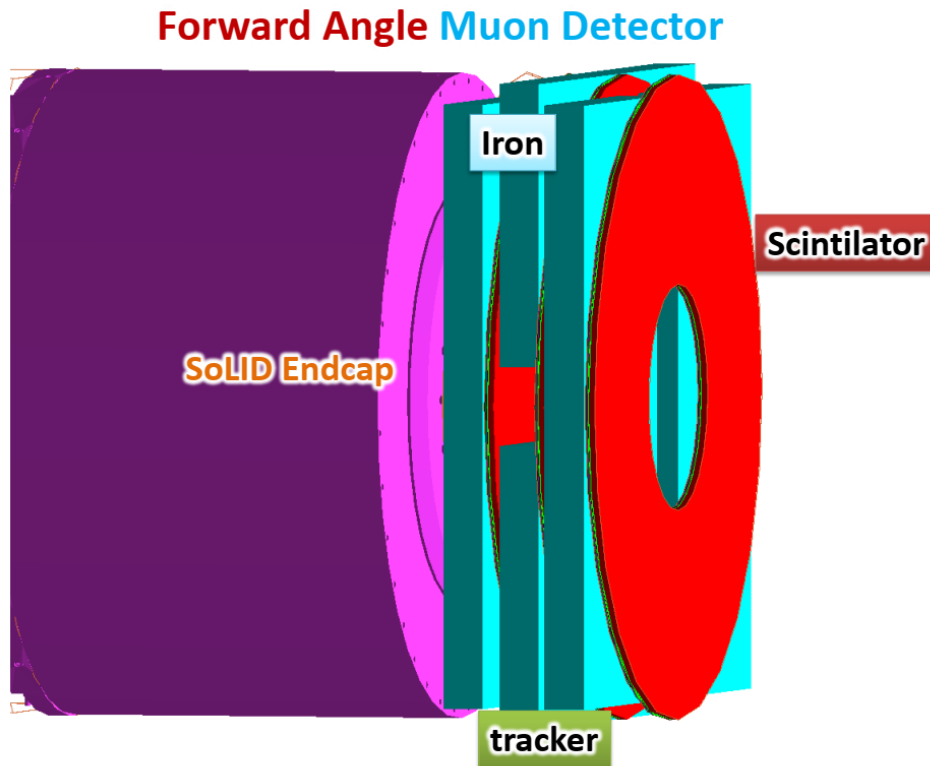
- Access to the real part of CFFs
- The Muon Charge Asymmetry (**μCA**), similar in nature to the forward-backward asymmetry of TCS, is predicted to have **significant amplitude** and rich **harmonic composition**
- Curvature sign change is a highly-discriminating feature for models
- **DDVCS μCA is dominated** by the CFF **H** and access a **CFF combination different** from **BSA**. This feature **distinguishes DDVCS** from DVCS and TCS

Experimental Setup



- Based on SoLID J/Psi and TCS setup with forward angle muon detector added to form SoLIDμ spectrometer
- Sharing beam time with added muon channels for J/Psi and TCS
- Forward Angle (FA) covers 8.5-16.5deg and Large Angle (LA) covers 18-30deg

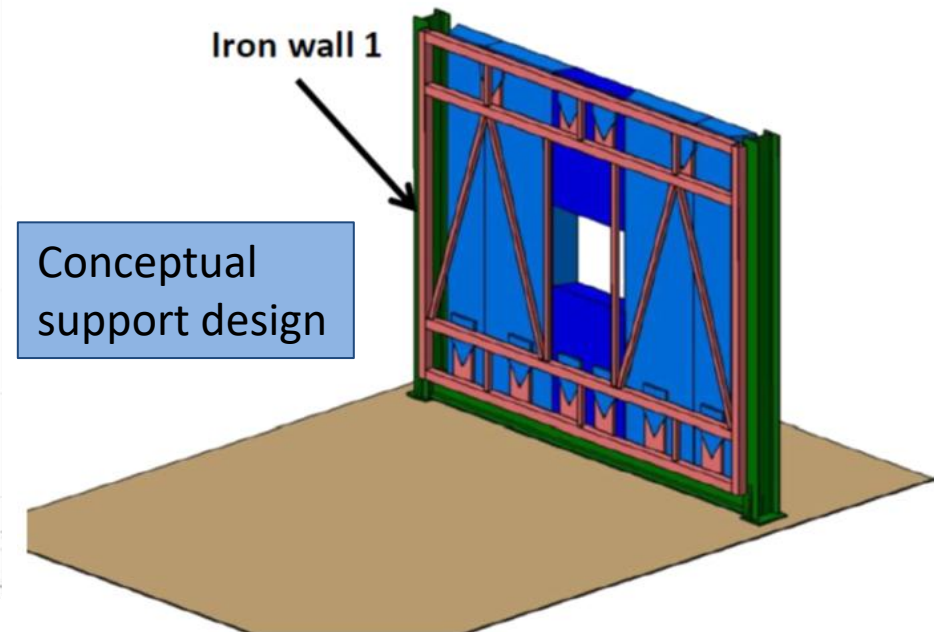
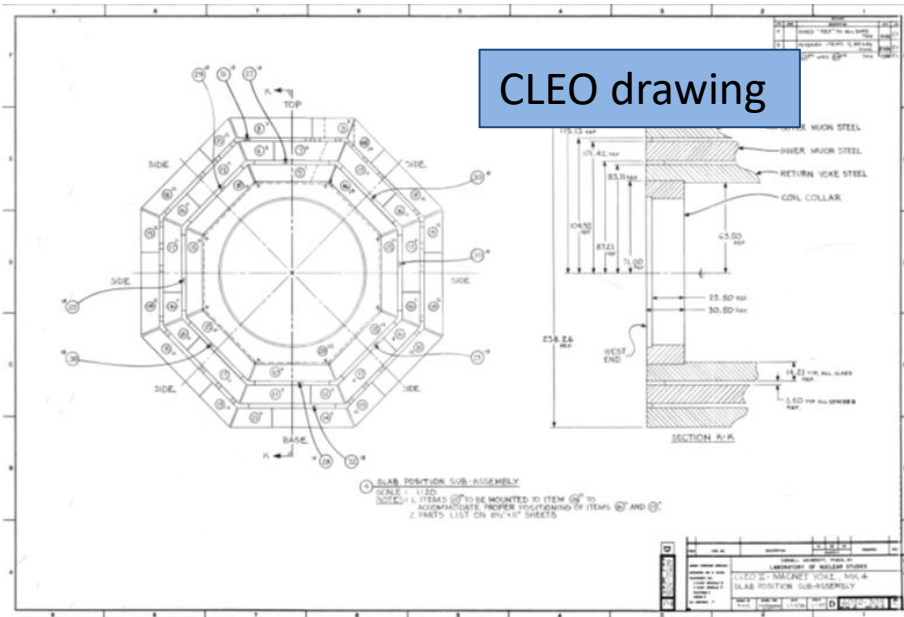
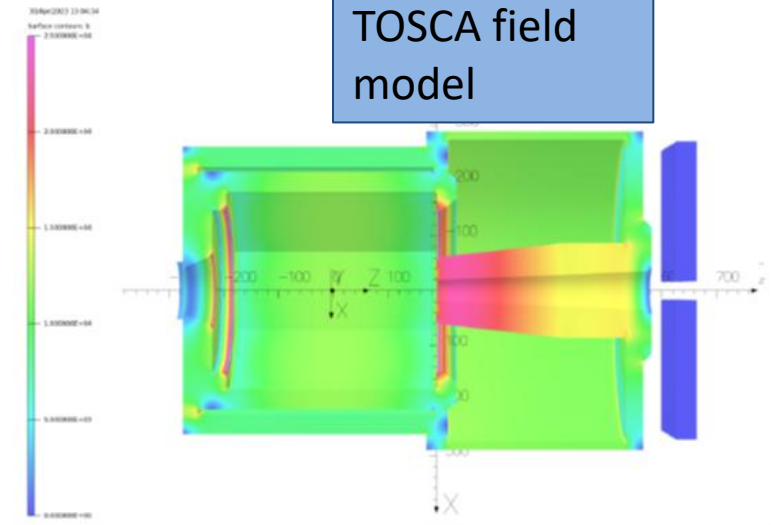
Forward Angle Muon Detector (FAMD)



- 3 layers of iron for pion blocking
- 3 layers of μ RWell trackers for tracks in FAMD to connect with tracks in SoLID inner GEM trackers
 - track resolution from SoLID inner trackers only
- 3 layers of scintillators for muon PID with pion suppression and for trigger

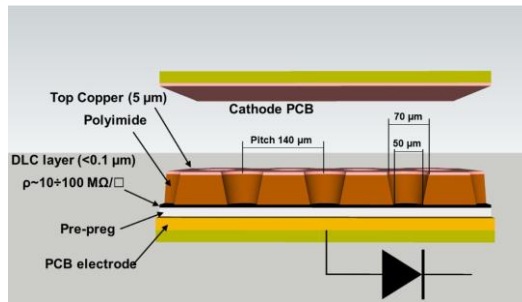
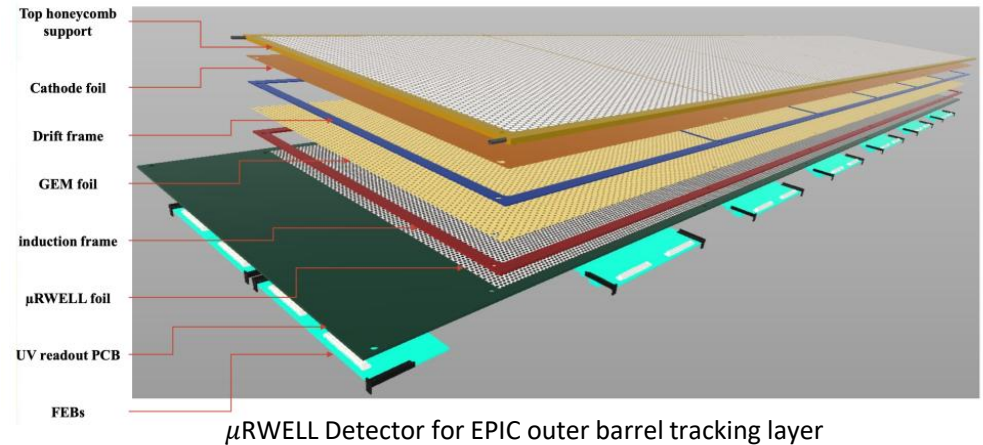
Iron of FAMD

- Reuse 6 of 8 CLEO octagon outer layer iron
- Each one is about 36x254x533cm
- No problem with space
- Field ($<10\text{G}$), force ($<1\text{N}$), torque ($<2\text{Nm}$) are small

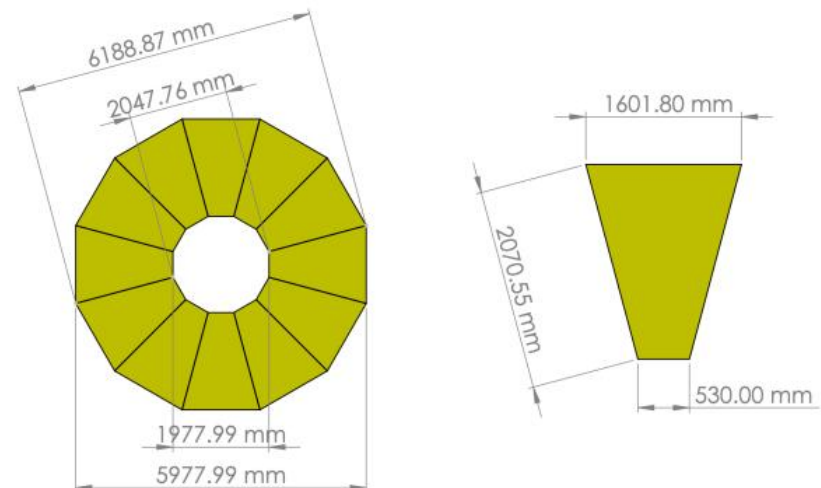


μ RWell trackers of FAMMD

- μ RWell with good rate capability and lower cost than GEM
- VMM electronics
- 2D UV strips with capacitive charge sharing to have rate 30KHz/cm² and position resolution of 1 mm



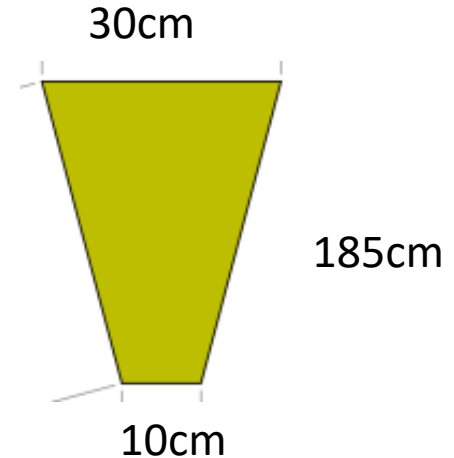
μ RWell Detector – G. Bencivenni *et al* 2019 *JINST* **14** P05014



A plane of μ RWell detectors for muon detection

Scintillators of FAMD

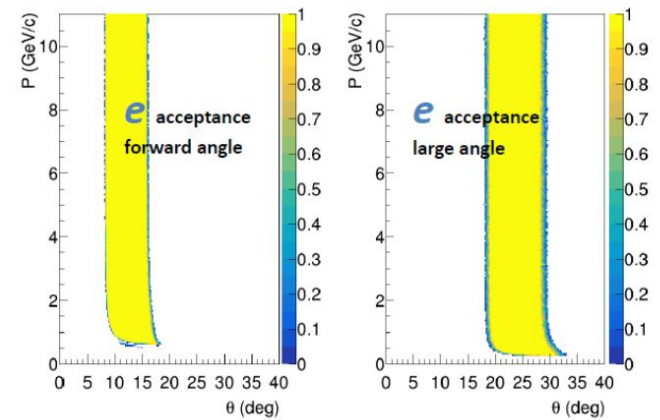
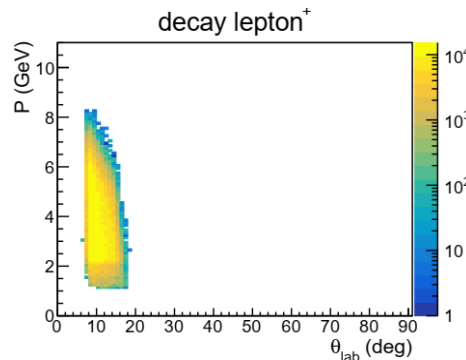
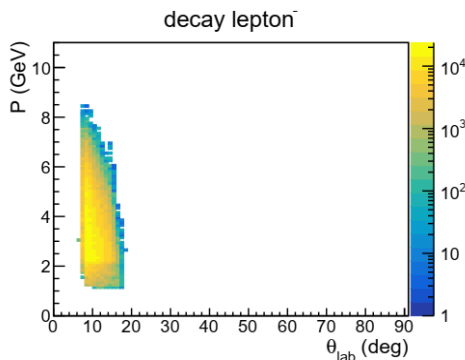
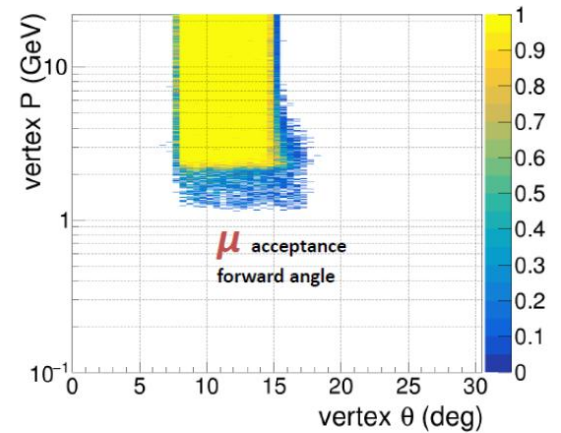
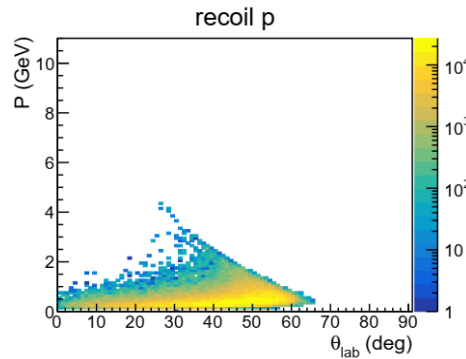
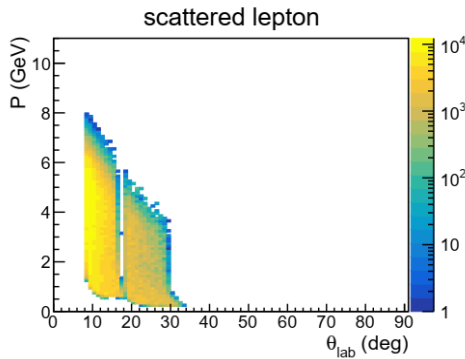
- Each plane has 60 azimuthal segments
- Readout with light guide and PMTs from both inner and outer radial ends
- Thickness 5cm and 150 ps time resolution
- Design similar to CLAS12 forward scintillator and SoLID large angle scintillator with similar performance



Event Acceptance

BH generator "grape-dilepton" used by HERA and verified by CLAS12

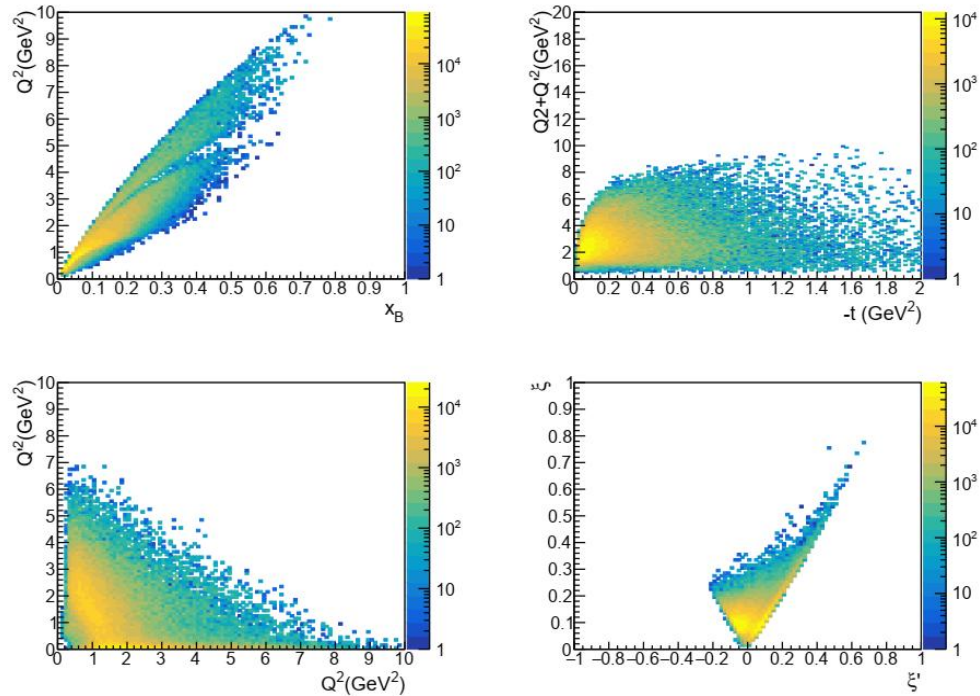
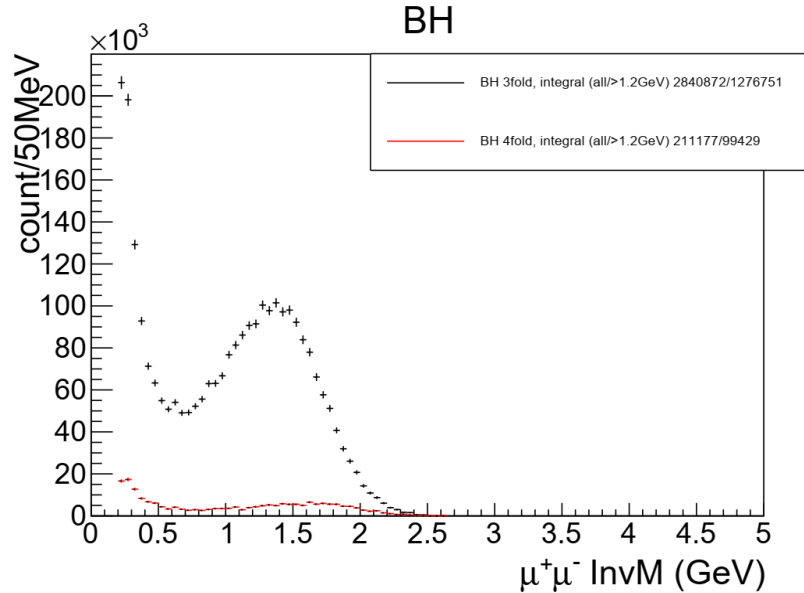
- Best topology 3fold(e+mu+mu): scattered e- at FA+LA, both muons at FA, proton not detected (shown below)
- Additional topology 4fold(e+mu+mu+p): scattered e- and recoil proton at FA+LA, both muons at FA



Event Distribution

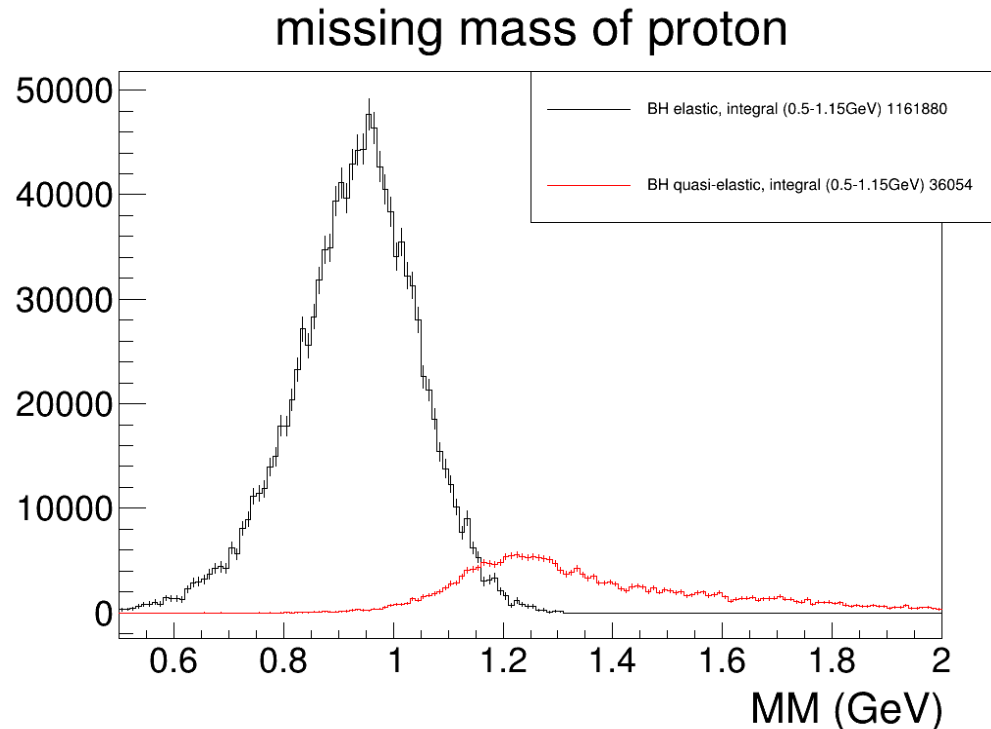
BH generator "grape-dilepton" used by HERA and verified by CLAS12

- 3fold BH events covers large kinematic range
- 0.7 overall detection efficiency
- Enough counts for $1.2 \times 10^{37}/\text{cm}^2/\text{s}$ lumi and 100 days to have multidimensional binning



Exclusivity cut

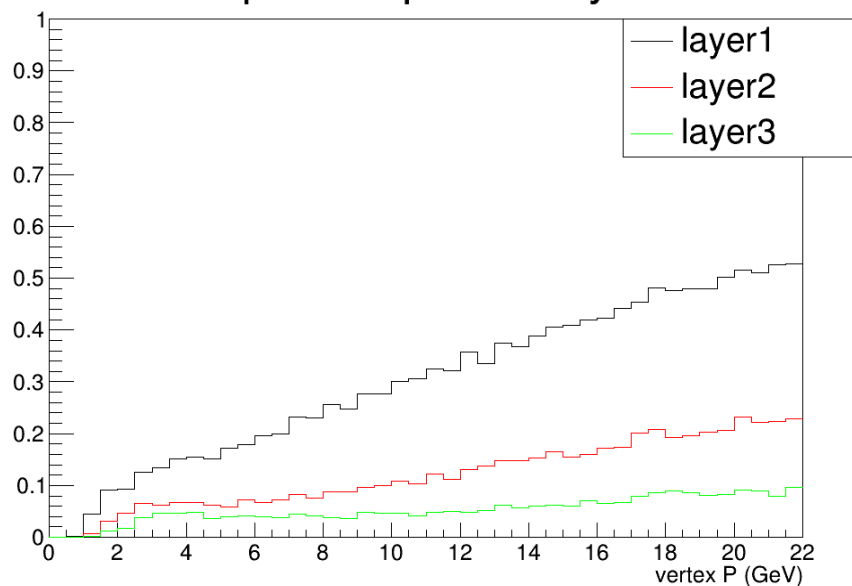
- Both BH with 4 final particles (elastic) and more than 4 particles (quasi-elastic) are generated by "grape-dilepton"
- Missing proton mass of 3 fold BH events with resolution from SoLID inner GEM trackers, for resonance free region (muon pair $\text{InvM} > 1.2 \text{ GeV}$)
- 3-4% background left after cutting $\text{MM} > 1.15 \text{ GeV}$



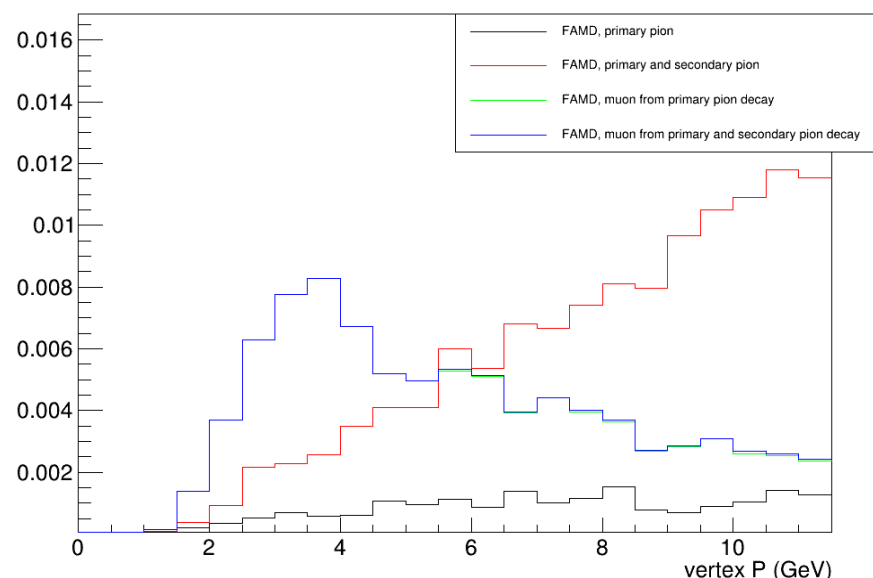
Pion blocking

- Geant4 simulation of pions from target with some probabilities creating hits at FAMD
- "pion hit probability", hits of charged particles entering each layer, used for FAMD detector and trigger rate estimate
- "pion surviving probability", hits of pion and muon at the last layer of FAMD and a track passing all SoLID inner GEM trackers, used for physics event rate estimation

pion hit probability

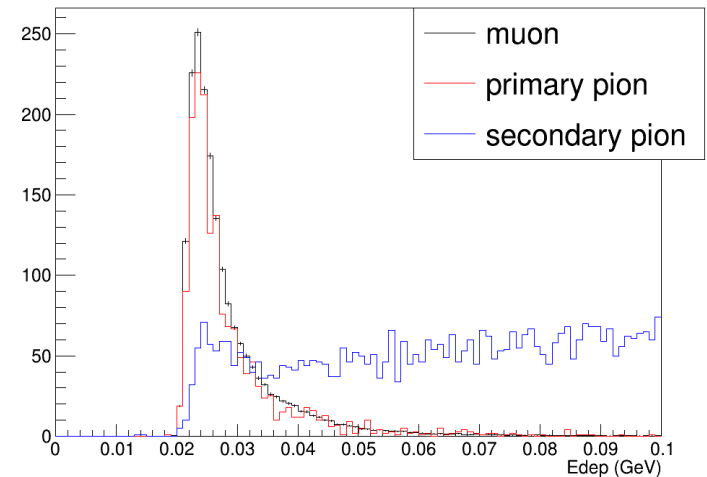
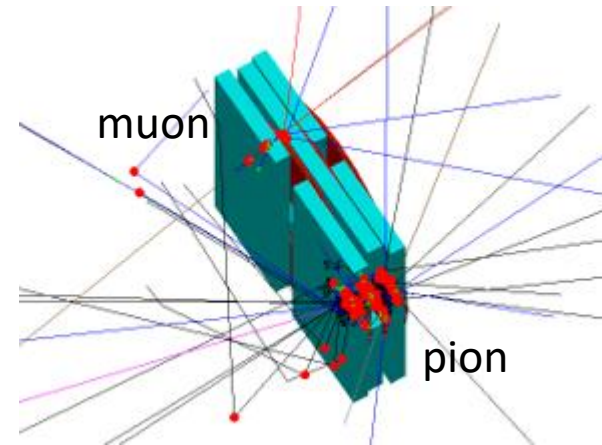


pion surviving probability



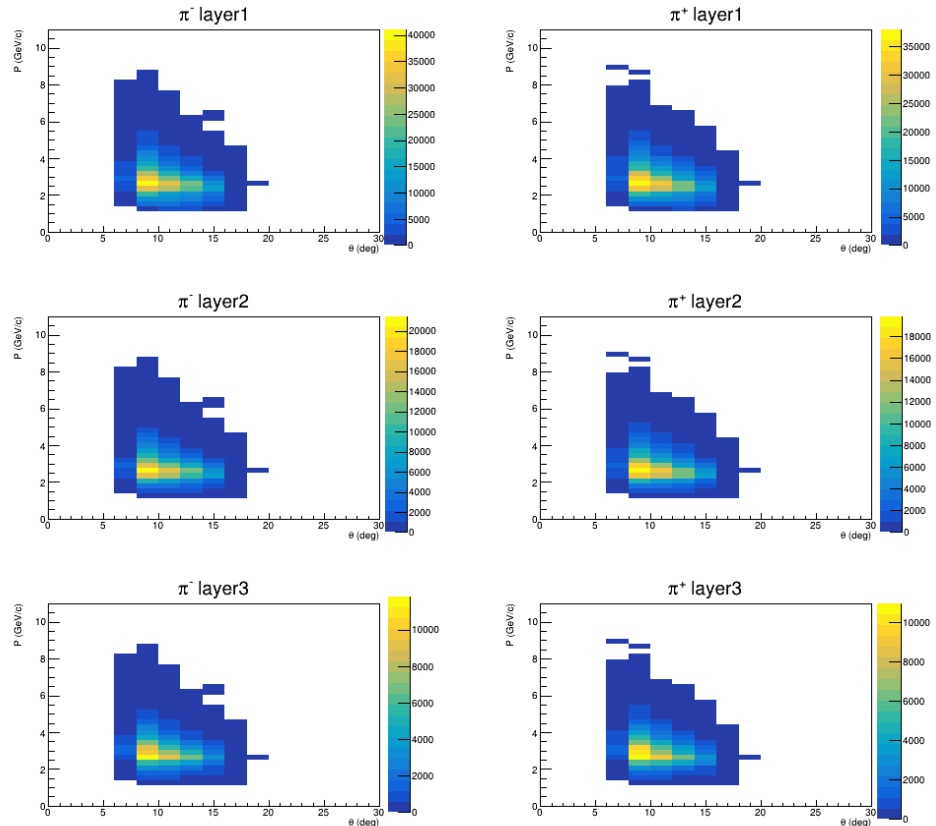
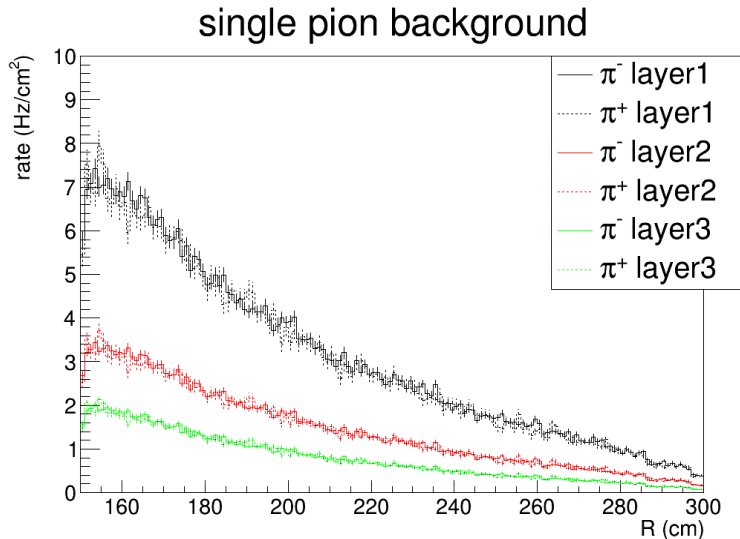
Pion suppression within FAMD

- Muons behave as Minimum Ionizing Particle (MIP)
- Pions often deposit more energy over 3 layers of scintillators.
- Use moderate pion suppression factor 2 from energy cut



Single pion background

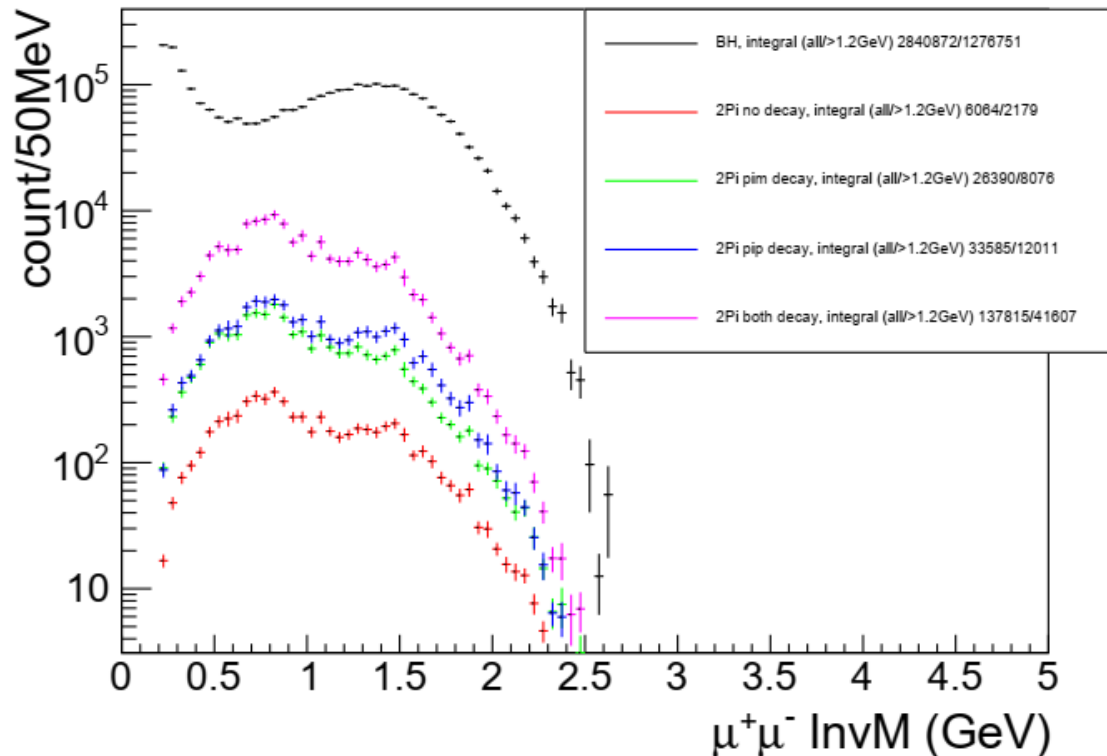
- Combining single pion generator "evgen_bggen" (pythia+MAID) events with "pion hit probability", study charged particle rate at 3 layers. Full simulation confirmed the result
- Single particle trigger 600khz rate with hits in all 3 layers of scintillators in nearby phi sectors
- Coincidence of two hits from 2 single particle trigger from 2 different phi sectors within 50ns time windows leads to 18khz final trigger rate
- Fake coin rate from single pion is below 1khz. BH di-muon events have two muons separated at least by 60 degrees in phi angle for the main physics region (muon pair $InvM > 1.2\text{GeV}$)



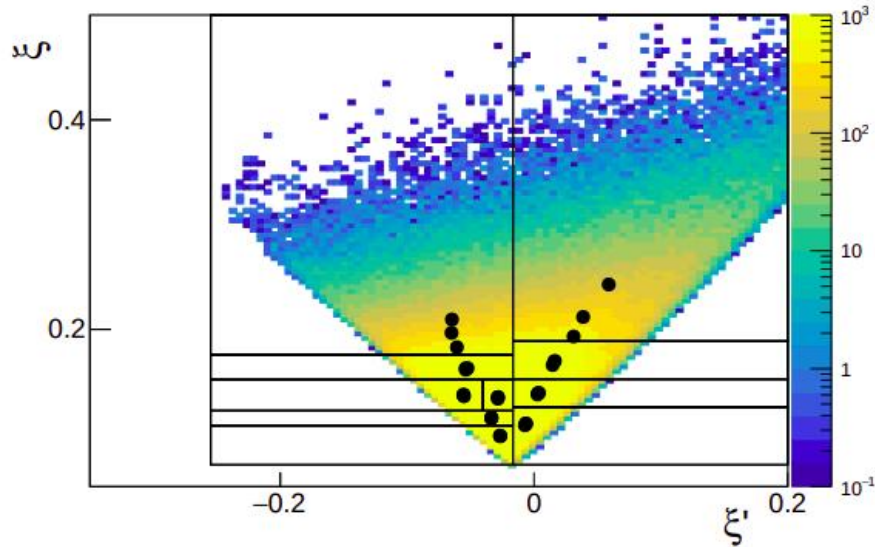
Two pion exclusive background

- Main physics background from two pion exclusive channel (missing mass cut won't reject it because pions and muons have similar mass)
- Combine event generator "twopeg" (fit to CLAS data) and "pion hit probability" with pion suppression factor 2, study "2pi" rate and compare to BH rate
- 5-7% background

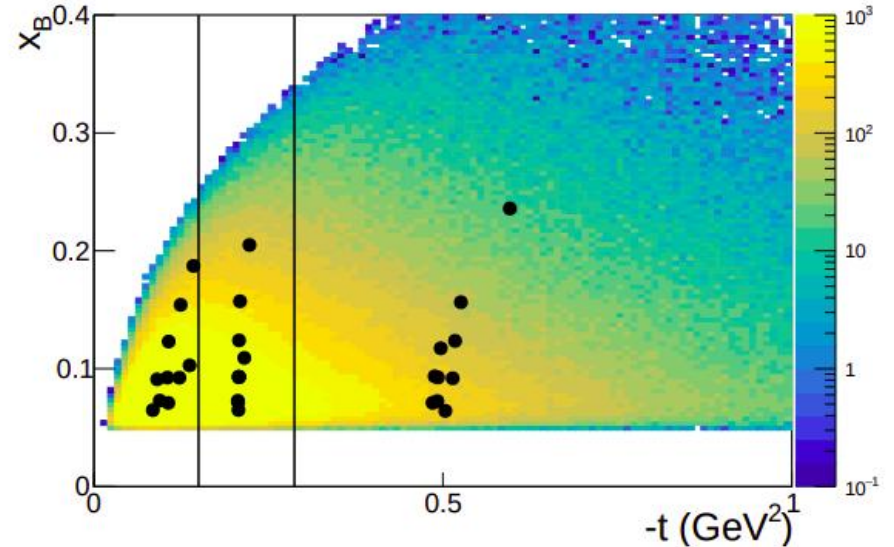
BH and 2pi comparison



Experimental projections



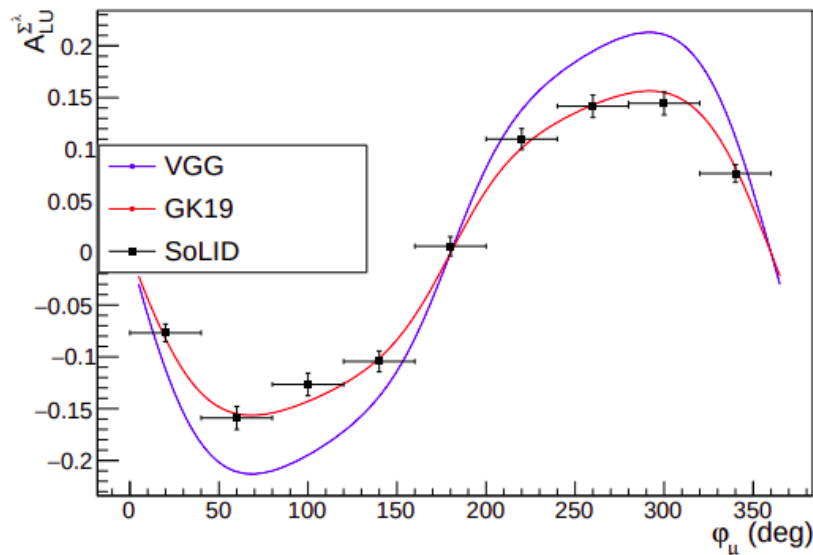
(a) (ξ', ξ) space.



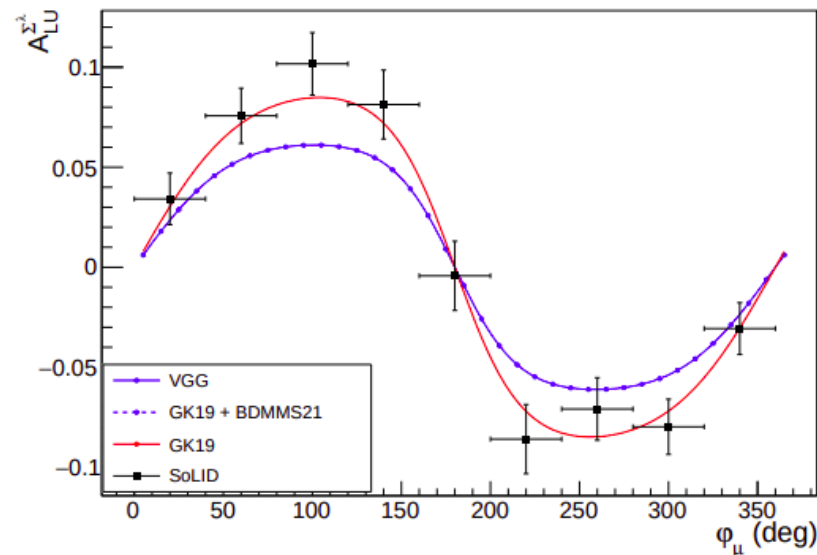
(b) $(-t, x_B)$ space.

- 100 days would allow for measurements on a five-dimensional grid

BSA experimental projections



(a) TCS-like BSA in the TCS-like region (Bin 21).

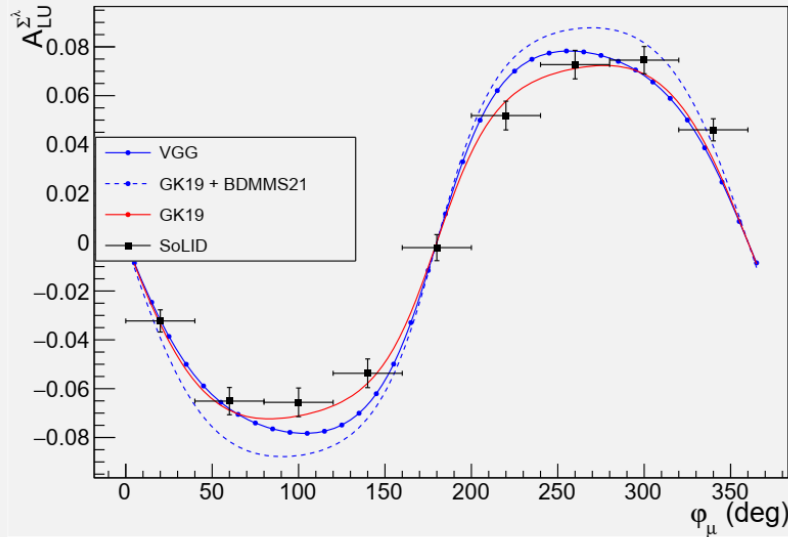


(b) TCS-like BSA in the full DVCS-like region.

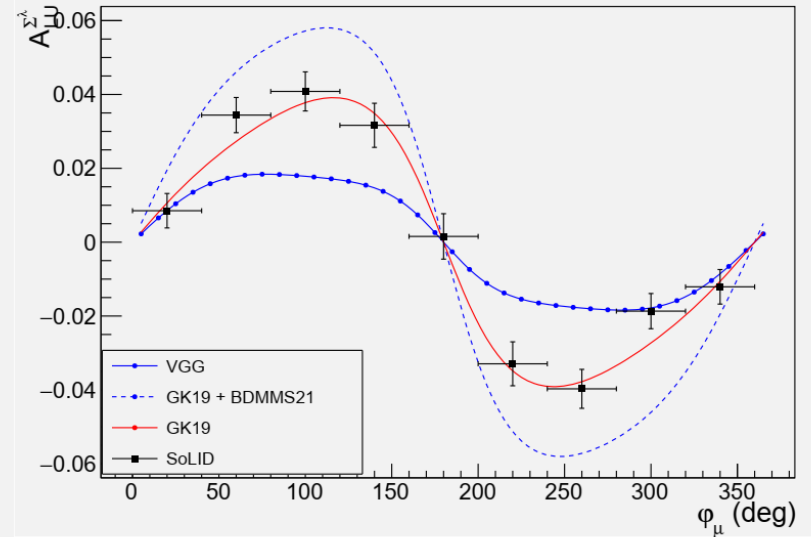
Figure 25: Sample TCS-like BSA projections.

- First time measurements of the BSA sign change
- Possibility to constrain GPD models

BSA experimental projections



(a) $-0.1 < \xi' < -0.04$.

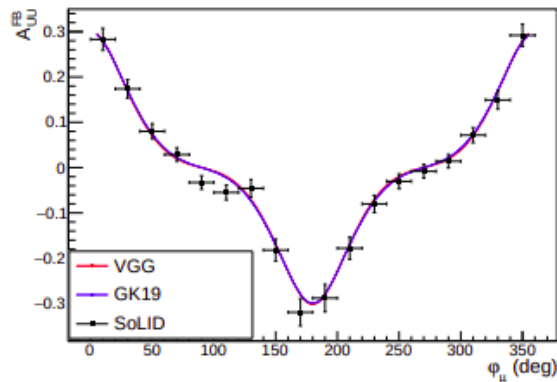


(b) $-0.04 < \xi' < 0.1$.

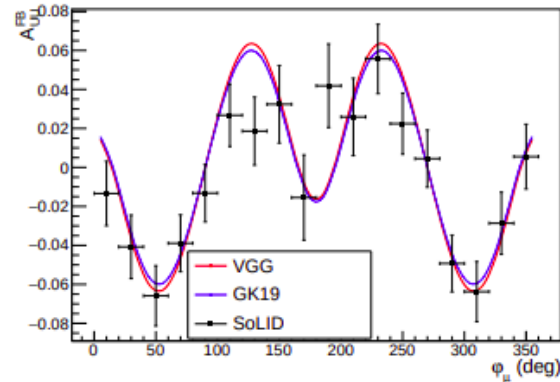
Figure 26: Projected exploratory TCS-like BSA measurements sensitive to shadow GPDs in the $0.3 < \xi < 0.4$ region.

- First-time exploratory measurement constraining shadow GPD models

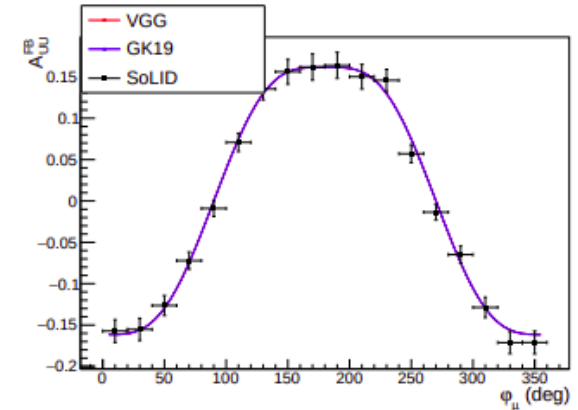
μ CA experimental projections



(d) Bin 19.



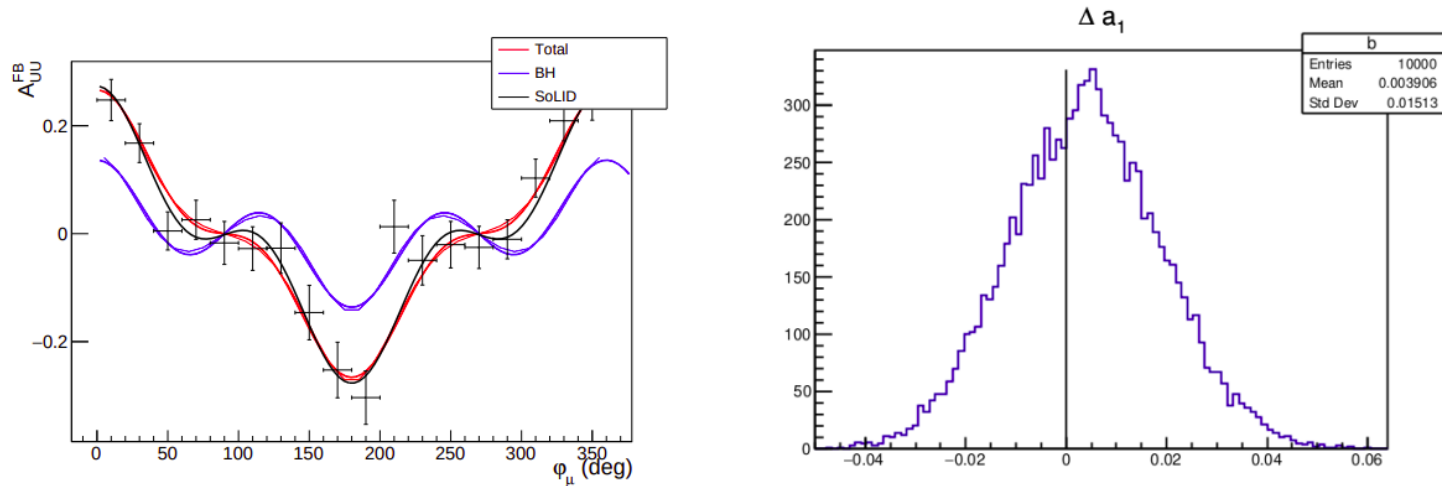
(e) Bin 20.



(f) Bin 21.

- Observation of the CFF real part with curvature change

μ CA experimental projections



(a) μ CA and the components entering the $\cos \varphi_\mu$ moment.

(b) Distribution of the $\cos \varphi_\mu$ moment of the μ CA after 10k iterations.

Figure 28: Extraction of $\cos \varphi_\mu$ moment of the μ CA on bin 13.

Sample $\cos(\phi)$ extraction with a 11% error

$$A_{UU}^{FB} = a_0 + a_1 \cos(\varphi) + a_3 \cos(3\varphi)$$

- μ CA has contributions from $\cos(\phi)$ and $\cos(3\phi)$ modulations
- $\cos(\phi)$ can be extracted from fits
- As BH is known, it can be subtracted

$$\frac{d^4\sigma_{INT}}{dQ^2 dt d\Omega} = -\frac{\alpha_{em}^3}{4\pi s^2} \frac{1}{-t} \frac{m_p}{Q'} \frac{1}{\tau\sqrt{1-\tau}} \frac{L_0}{L} [\cos(\phi) \frac{1+\cos^2(\theta)}{\sin(\theta)} \text{Re}\tilde{M}^{--} - \cos(2\phi) \sqrt{2} \cos(\theta) \text{Re}\tilde{M}^{0-} + \cos(3\phi) \sin(\theta) \text{Re}\tilde{M}^{+-} + O(\frac{1}{Q'})],$$

Systematic effects

The definition of experimental observables at the **5-fold differential** level is required to **compensate** the **cross-section smallness** and to **minimize** the contribution of the **BH₂** process

$$A_{LU}^{\Sigma\lambda} = \frac{1}{\lambda} \frac{Y_+ - Y_-}{Y_+ + Y_-}$$

$$Y_{\pm}(\varphi_{\mu}) = \frac{1}{Q_{\pm}} \frac{1}{\Delta\Omega_e(\varphi_{\mu}) \Delta\theta_{\mu}(\varphi_{\mu})} \int_0^{2\pi} d\phi \int_{\pi/4}^{3\pi/4} d\theta_{\mu} \sin(\theta_{\mu}) \frac{N_{\pm}(\varphi_{\mu}, \phi, \theta_{\mu})}{\epsilon_e(\phi) \epsilon_{\mu}(\varphi_{\mu}, \theta_{\mu})}$$

$$A_{UU}^{\mu\pm} = \frac{Y^+ - Y^-}{Y^+ + Y^-}$$

$$Y^{\pm}(\varphi_{\mu}) = \frac{1}{\Delta\Omega_e(\varphi_{\mu}) \Delta\theta_{\mu^{\pm}}(\varphi_{\mu})} \int_0^{2\pi} d\phi \int_{\pi/4}^{3\pi/4} d\theta_{\mu} \sin(\theta_{\mu}) \frac{N^{\pm}(\varphi_{\mu}, \phi, \theta_{\mu})}{\epsilon_e(\phi) \epsilon_{\mu^{\pm}}(\varphi_{\mu}, \theta_{\mu})}$$

- **BSA systematics** originates from the knowledge of : the **electron beam polarization**, the **electron detection efficiency**, and the **muon detection efficiency**.
- **μCA systematics** originates from the knowledge of : the **electron detection efficiency**, the **muon detection efficiency**, and the **muon solid angle**.

Systematic effects

- Systematics of the measurements will be controlled via **simulations** and the measurement of **reference processes**. The **solenoidal field** and the **symmetrical configuration** of SoLID μ offer further cross-checks
- **Muon solid angle** : extensive simulations based on the **SoLID μ GEANT4 model** ($\delta\Delta\theta_\mu/\Delta\theta_\mu \sim 3\%$)
- **Electron detection efficiency** : measurement of **DIS** and **elastic** electron **scattering** ($\delta\epsilon_e/\epsilon_e \sim 7\%$)
- **Muon detection efficiency** : measurement of **Bethe-Heitler** and comparison of the e^\pm and μ^\pm **decay** of specific meson ($\phi, J/\Psi$) ($\delta\epsilon_\mu/\epsilon_\mu \sim 15\%$)

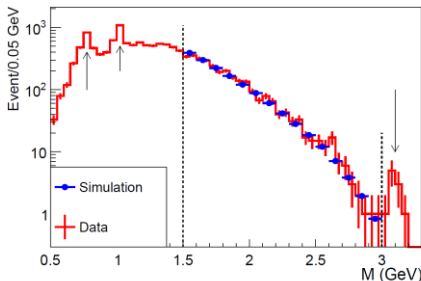
Bin independence hypothesis

$$Y_\pm(\varphi_\mu) \equiv \sum_{i=1}^{N_\phi} \sum_{j=1}^{N_{\theta_\mu}} \frac{n_\pm^{ij}}{\epsilon_e^i \epsilon_\mu^j} \quad \delta A_{LU}^{\Sigma\lambda} = \sqrt{\left[A_{LU}^{\Sigma\lambda}\right]^2 \left(\frac{\delta\lambda}{\lambda}\right)^2 + \frac{1}{2\lambda^2} \frac{1}{N_\phi} \left(\frac{\delta\epsilon_e}{\epsilon_e}\right)^2 + \frac{1}{2\lambda^2} \frac{1}{N_{\theta_\mu}} \left(\frac{\delta\epsilon_\mu}{\epsilon_\mu}\right)^2} \rightarrow 0.04$$

$\lambda = 0.85$

$$Y^\pm(\varphi_\mu) \equiv \frac{1}{\Delta\theta_{\mu^\pm}} \sum_{i=1}^{N_\phi} \sum_{j=1}^{N_{\theta_\mu}} \frac{n_{ij}^\pm}{\epsilon_e^i \epsilon_{\mu^\pm}^j} \quad \delta A_{UU}^{\mu^\pm} = \sqrt{\left(\frac{\delta\Delta\theta_\mu}{\Delta\theta_\mu}\right)^2 + \frac{1}{N_\phi} \left(\frac{\delta\epsilon_e}{\epsilon_e}\right)^2 + \frac{1}{N_{\theta_\mu}} \left(\frac{\delta\epsilon_\mu}{\epsilon_\mu}\right)^2} \rightarrow 0.06$$

(N_ϕ, N_{θ_μ}) are the kinematic dependent number of bins, typically (20,10)



- CLAS12 di-e data and sim of BH in resonance free region are used to check absolute efficiency and its error.
- GlueX has done similar thing
- SoLID μ should use both resonance and resonance free region and cross check both di-e and di-mu channels to **help systematics study**

Beam time request

Beam Energy (GeV)	Beam Current (uA)	Beam Requirements	Target Material	Target Thickness (cm)	Beam time (days)
11	3	polarized (>85%)	LH2	15	
Run Group Calibration time					10
Run Group Production time					50
Requested Production time					50
Total Time					110

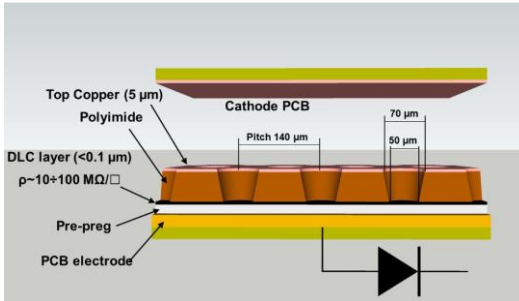
- Only trigger on di-muon to take DDVCS, J/Psi and TCS di-mu data at the same time
- Independent di-e data taking happening at the same time

Summary

- complement SoLID J/Psi setup with a forward angle muon detector to form **SoLID μ spectrometer**
- measure DDVCS in the di-muon channel
- use the J/Psi beamtime 60 days and request additional 50 days
- **first time measurement** of DDVCS (mainly BSA, and exploratory μ CA) over a broad kinematic range
- **first time to access GPD** $|x| < \xi$ as input for models
- J/Psi and TCS will have additional di-muon data and more di-e data

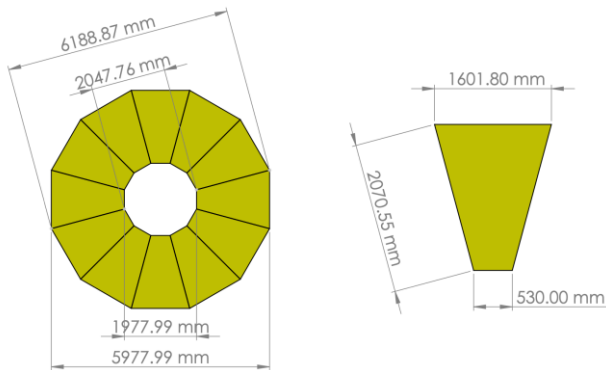
Backup

Muon Detector Tracker

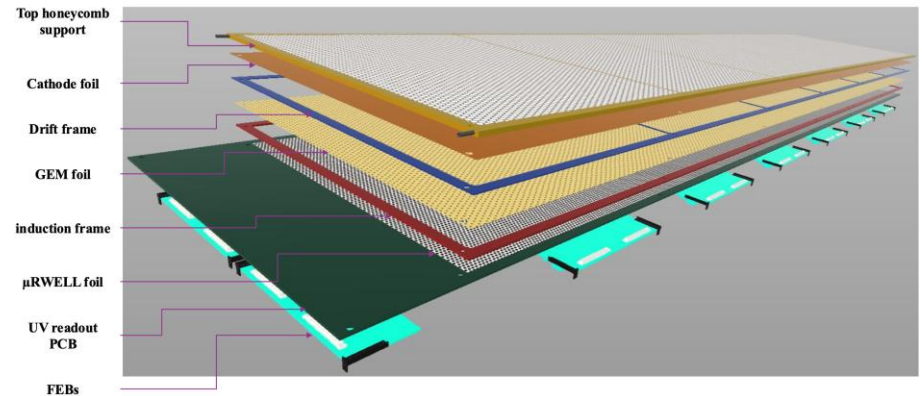


- Utilize μ RWELL detectors for muon tracking layers
 - Current μ RWELL detector rate capability – $\sim 200 \text{ KHz/cm}^2$ (High-rate version in development – 10 MHz/cm^2)
 - Discharge resistant thanks to integrated DLC layers – a huge improvement on electronics stability – less interruption on DAQ during running
 - No spacers needed compared with GEM detectors – no dead area
- A similar technology adopted by EIC
 - Our muon detector unit would be roughly in the same size as EIC prototypes
 - Total cost (3 complete layers covering a total of 75 m^2) around 900K

μ RWELL Detector – G. Bencivenni *et al* 2019 *JINST* **14** P05014



A plane of μ RWELL detectors for muon detection



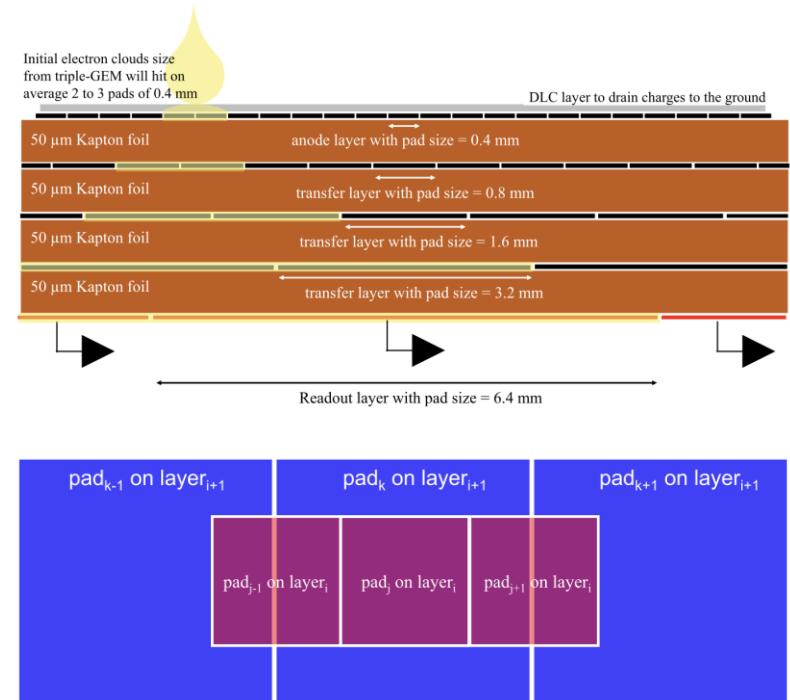
μ RWELL Detector for EPIC outer barrel tracking layer

Muon Detector Tracker

- Use **capacitive charge sharing** technique to reduce total readout channels while maintain the **same space resolution**
- Works for all readout patterns – strip, pad, zigzag, ...

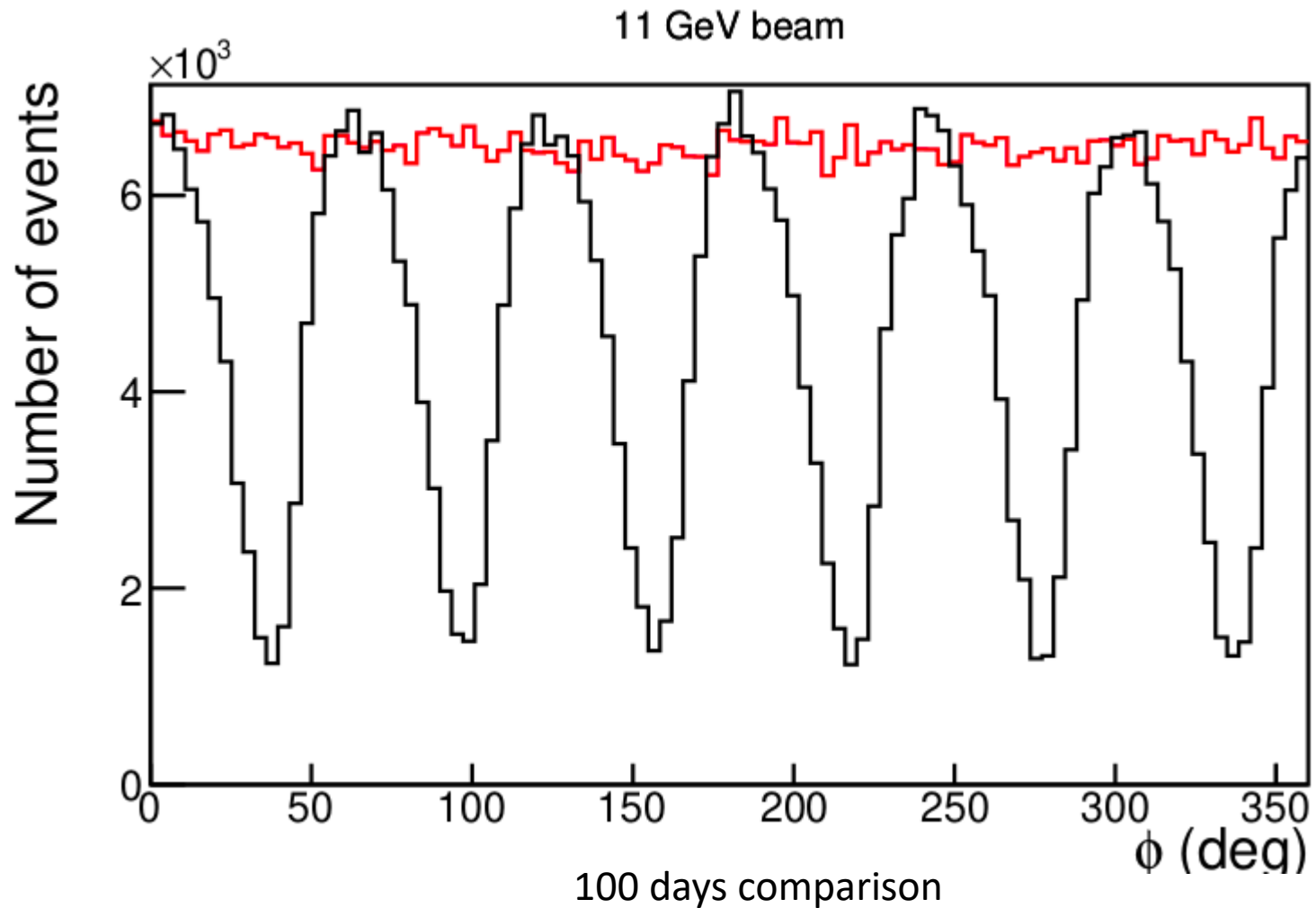
With Capacitive charge sharing:

- Space resolution : 1 mm
- Total readout channel can be reduced to around 22K for all 3 layers combined
- Detector rate will be determined by the final readout strip width, larger strip width leads to lower detector rate capability
- For 22K readout channels, 1 mm space resolution, with capacitive charge sharing technique – **rate capability: $\sim 30 \text{ KHz/cm}^2$** (assume 300 ns signal integral time)

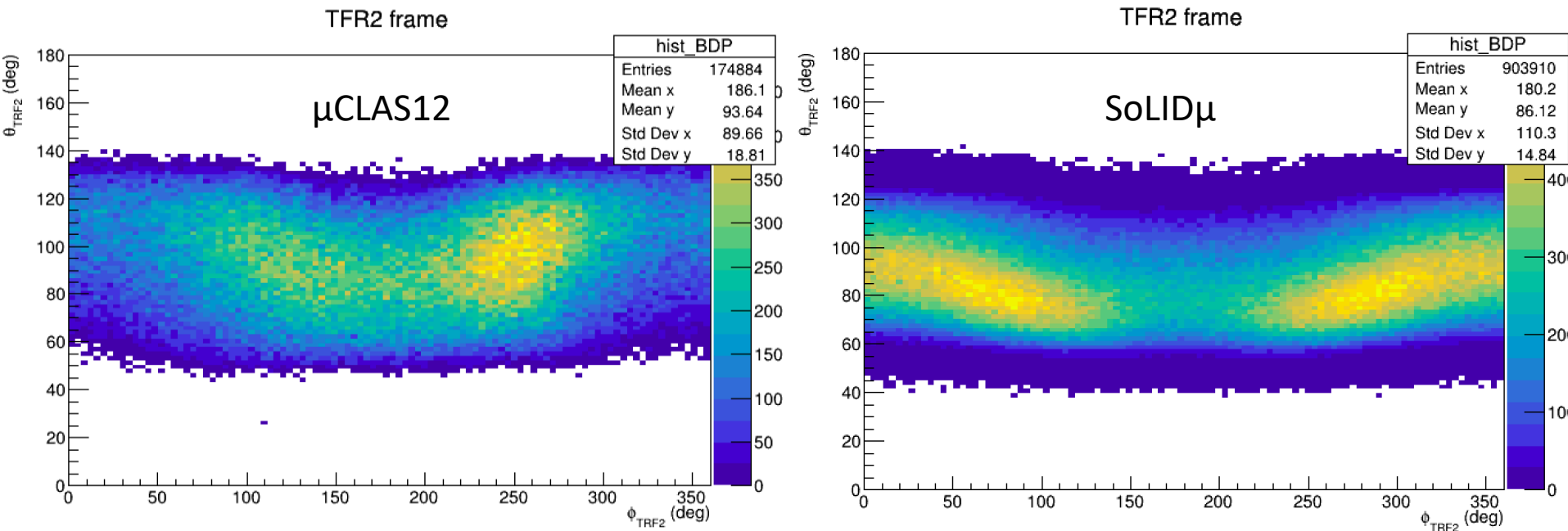


Concept for capacitive charge sharing – K. Gnanvo *et al*, *Nuclear Inst. and Methods in Physics Research, A* 1047 (2023) 167782

SoLID μ vs μ CLAS12



SoLID μ vs μ CLAS12



- Angles in the muon center-of-mass frame
- Larger coverage with SoLID μ

Cost

System	Item	Cost (K\$)
Tracker planes	uRWell	900
	VMM readout	300
	HV	10
	Mechanical	100
Scintillator planes	Scint. materials	640
	light guide	180
	PMT+base	180
	FADC	500
	HV	150
	Mechanical	100
Iron planes	Mechanical	200
Total		3,260

Table 1: Cost estimation of the forward angle muon detector and related hardware.

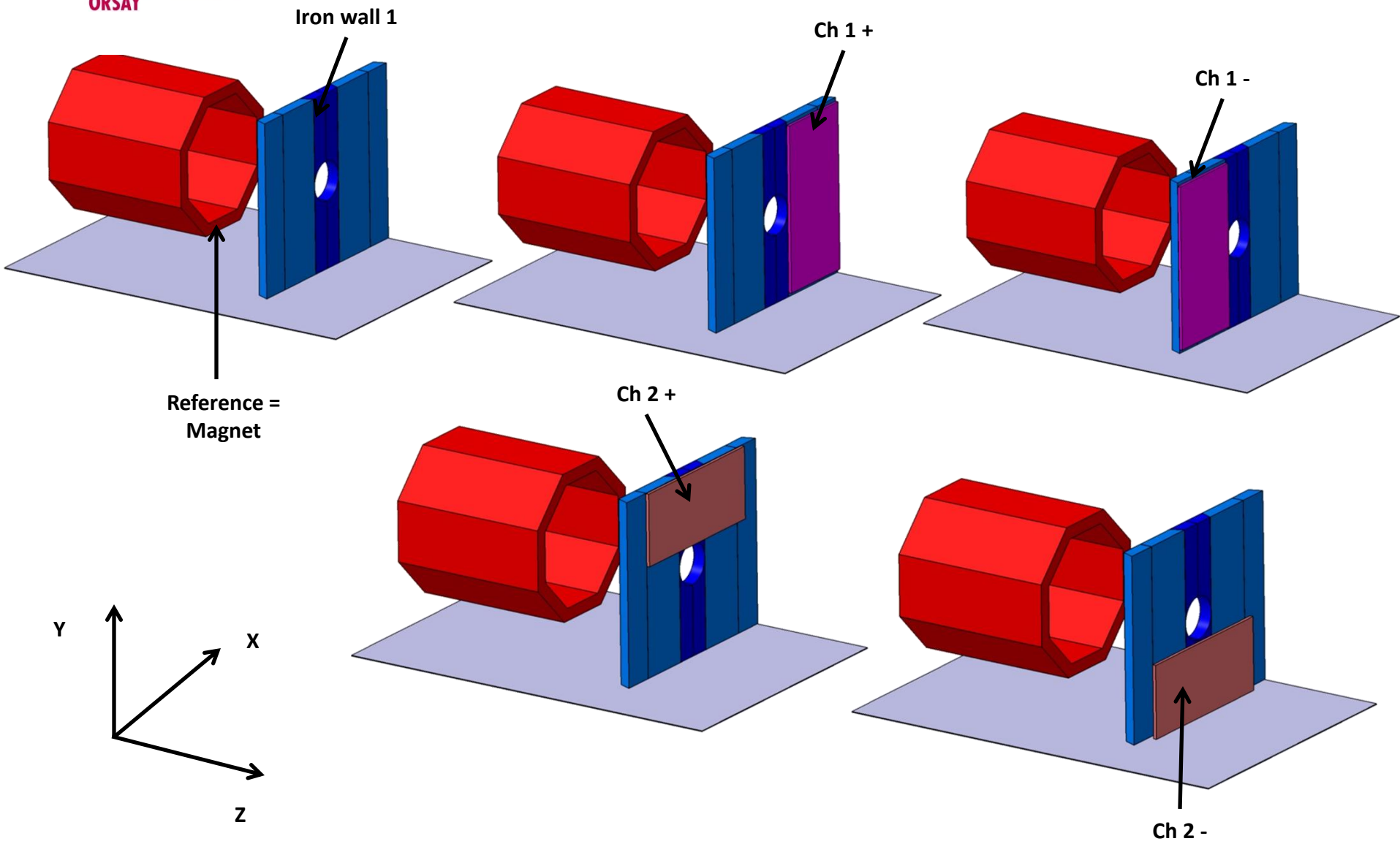
Binning

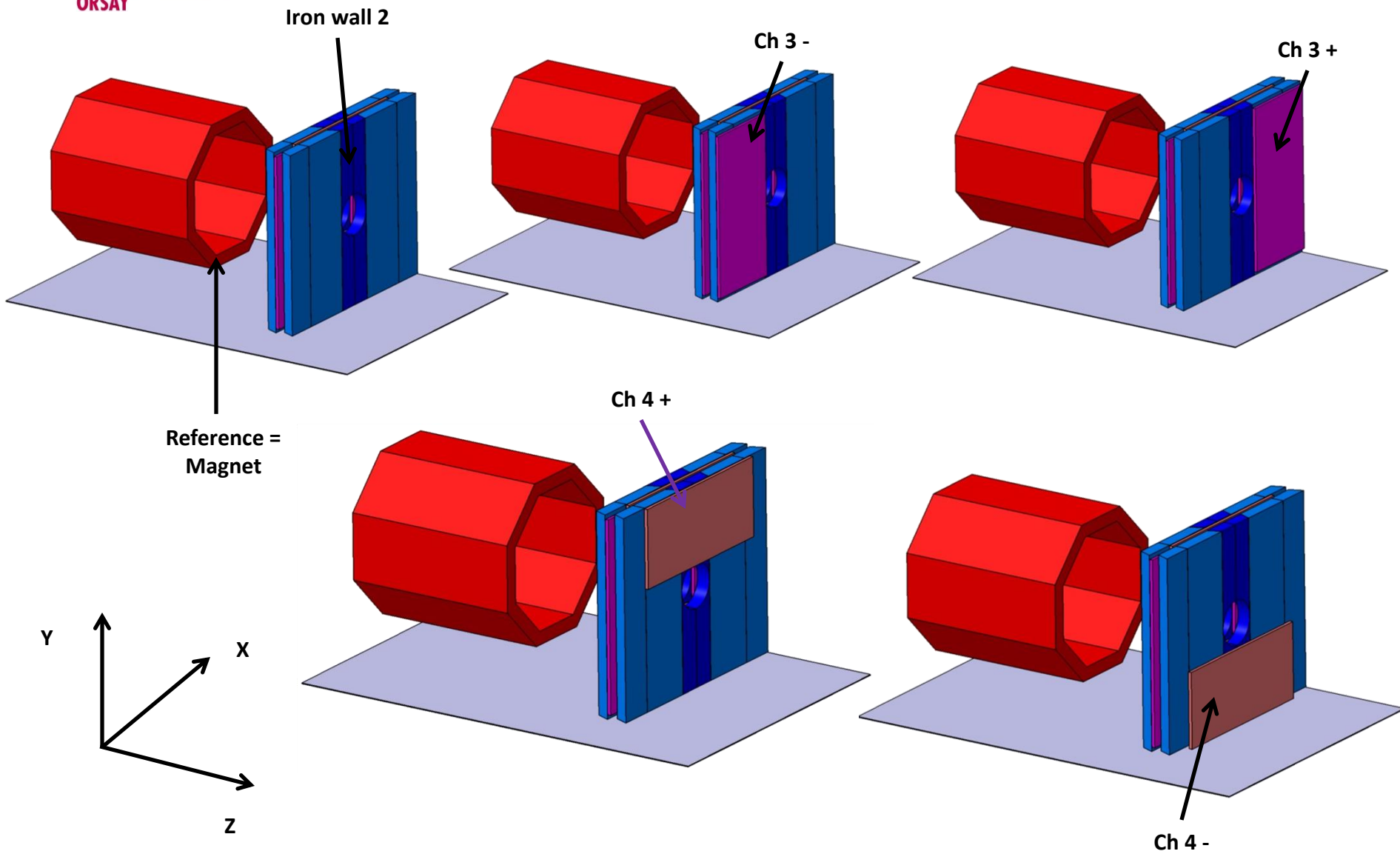
Bin	ξ' range	ξ range	t range (GeV ²)
1	$-0.255 < \xi' < 0$	$0.152 < \xi < 0.176$	$-5.541 < t < -0.287$
2			$-0.287 < t < -0.150$
3			$-0.150 < t < -0.020$
4		$0.176 < \xi < 0.739$	$-5.541 < t < -0.287$
5			$-0.287 < t < -0.150$
6			$-0.150 < t < -0.020$
7	$0 < \xi' < 0.512$	$0.071 < \xi < 0.126$	$-5.541 < t < -0.287$
8			$-0.287 < t < -0.150$
9			$-0.150 < t < -0.020$
10		$0.126 < \xi < 0.153$	$-5.541 < t < -0.287$
11			$-0.287 < t < -0.150$
12			$-0.150 < t < -0.020$
13		$0.153 < \xi < 0.189$	$-5.541 < t < -0.287$
14			$-0.287 < t < -0.150$
15			$-0.150 < t < -0.020$
16		$0.189 < \xi < 0.739$	$-5.541 < t < -0.287$
17			$-0.287 < t < -0.150$
18			$-0.150 < t < -0.020$
19	$-0.255 < \xi' < -0.017$	$0.071 < \xi < 0.108$	$-5.541 < t < -0.287$
20			$-0.287 < t < -0.150$
21			$-0.150 < t < -0.020$
22		$0.108 < \xi < 0.122$	$-5.541 < t < -0.287$
23			$-0.287 < t < -0.150$
24			$-0.150 < t < -0.020$
25	$-0.255 < \xi' < -0.040$	$0.122 < \xi < 0.152$	$-5.541 < t < -0.287$
26			$-0.287 < t < -0.150$
27			$-0.150 < t < -0.020$
28	$-0.040 < \xi' < -0.017$	$0.122 < \xi < 0.152$	$-5.541 < t < -0.287$
29			$-0.287 < t < -0.150$
30			$-0.150 < t < -0.020$

Table 2: Bin boundaries of the binning scheme shown in Fig. [24](#).

TAC report

1. This proposal will use SoLID with addition of 3-layers of muon detectors, which reuse the iron plates from CLEO (now at JLab) with new tracking detectors and scintillators. Part of the running (10 days calibration, 50 days production) is parasitic to the approved SoLID-J/psi (E12-12-006) experiment and additional 50 days beam time is requested.
2. The proposed measurement, aiming for a first dedicated precision DDVCS measurement, will also enhance the approved SoLID-J/psi and TCS measurements.
3. The J/psi configuration of the SoLID setup has gone through several JLab/DOE reviews and prototype tested with pre-R&D activities. The muon detector is a new design with its performance simulated. A rough estimation of cost was provided.
4. When estimating the additional trigger rate from “di-muon” events (18KHz) it was assumed that the two single rates in 3rd layer are uncorrelated and that a 50 ns time window was used to obtain the accidental coincidence rate. However, there could be single surviving pion/muon events with a correlated additional hit (secondary particle from single pion/muon hitting materials before 3rd layer and then the secondary particle producing a hit in 3rd layer in coincidence with the single pion/muon event). These type of “di-muon” events will not be reduced by the 50 ns window. Is there an estimate of the rate of these correlated two-hit events that would be included in the “di-muon” trigger rate?
5. To not be overwhelmed by low energy electrons, the J/psi trigger has ECal threshold cuts. The acceptance plots (figures 14-16) seem to not have the low momentum limits corresponding to the ECal threshold cuts. Are the physics projections corresponding to the acceptance of these plots or the acceptance with ECal trigger cuts?
6. The control of systematics of the detector efficiency and acceptance needs more careful study. Simulations alone will not be enough. Calibrations with measurements of specific physics channels may work well for the electron detection, but not clear how well they will work for the muon detector. No clear justifications were given for the “worst case scenario” or the “more reasonable case” (page 37).





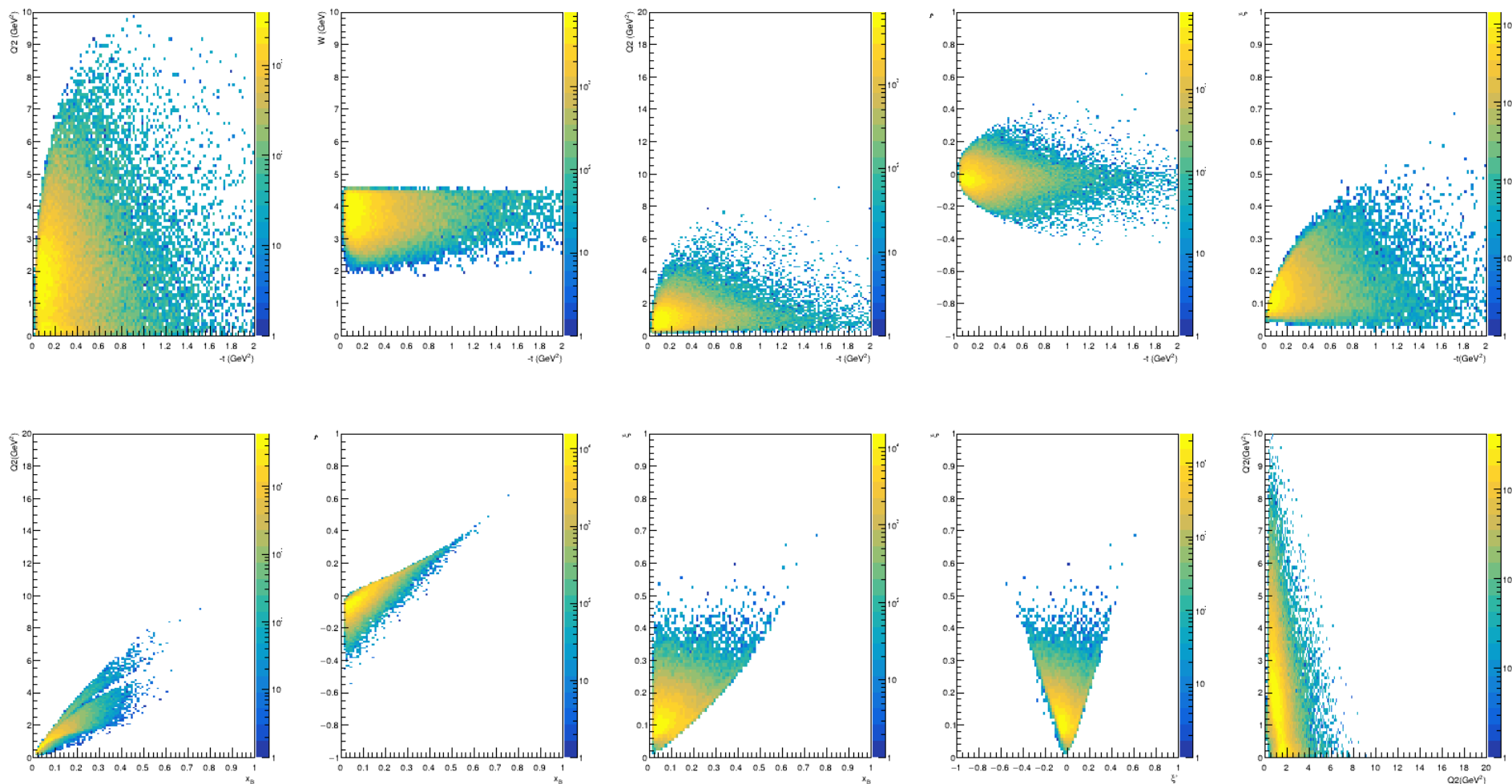
Higher luminosity ?

- Current could go up to 80 uA
- Target length up to 1 meter ($\sim 1.8 \cdot 10^{39} \text{ cm}^{-2}\text{s}^{-1}$)
- Tracker occupancy and photon background
 - Reduce amount of Copper in GEM
 - Micromegas option
 - Build smaller chambers and add more channels
 - Study complement with 2D pad readout
 - Superconducting tracker option
 - Radiation hardened silicon and MAPS
- Calorimetry
 - Study liquid scintillator and cryogenics calorimeter option
 - Superconducting detector to replace PMT (1 ns width pulse to increase rate capability)
- Cerenkov
 - Superconducting detector to replace PMT (1 ns width pulse to increase rate capability)
 - HBD type Cerenkov for Large Angle calorimeter

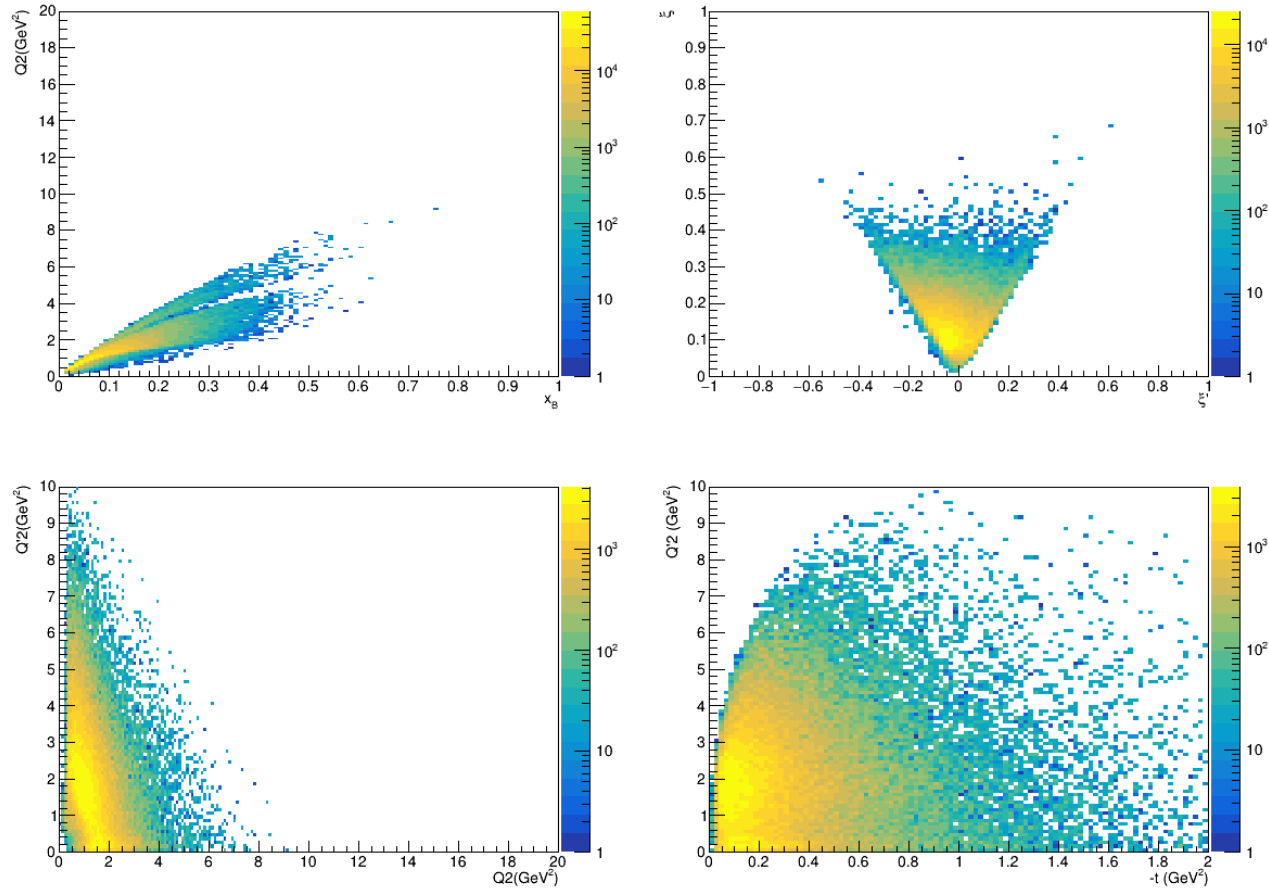
6. $10^{38} \text{ cm}^{-2}\text{s}^{-1}$

Technically doable mostly matter of cost

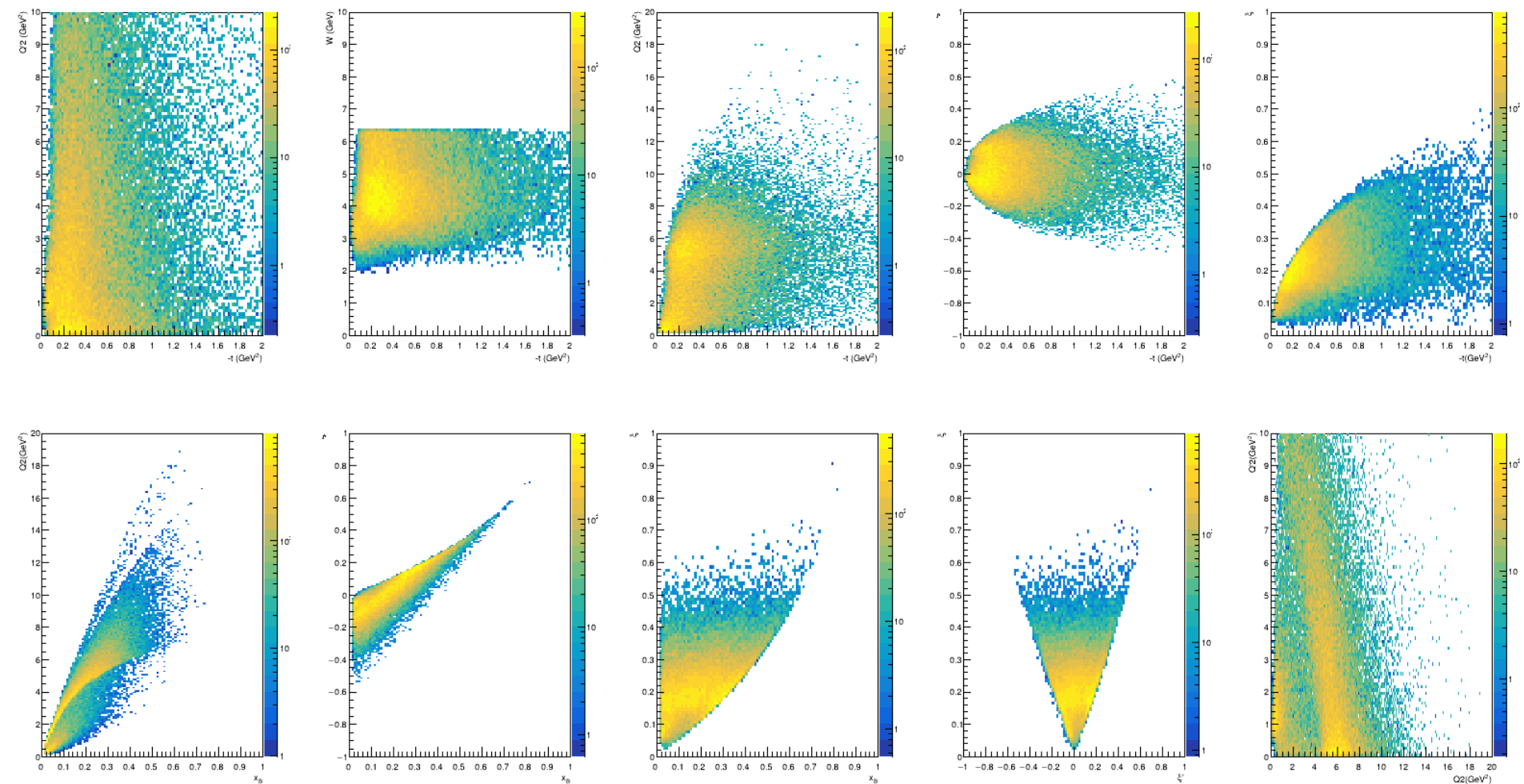
Kinematical coverage 11 GeV



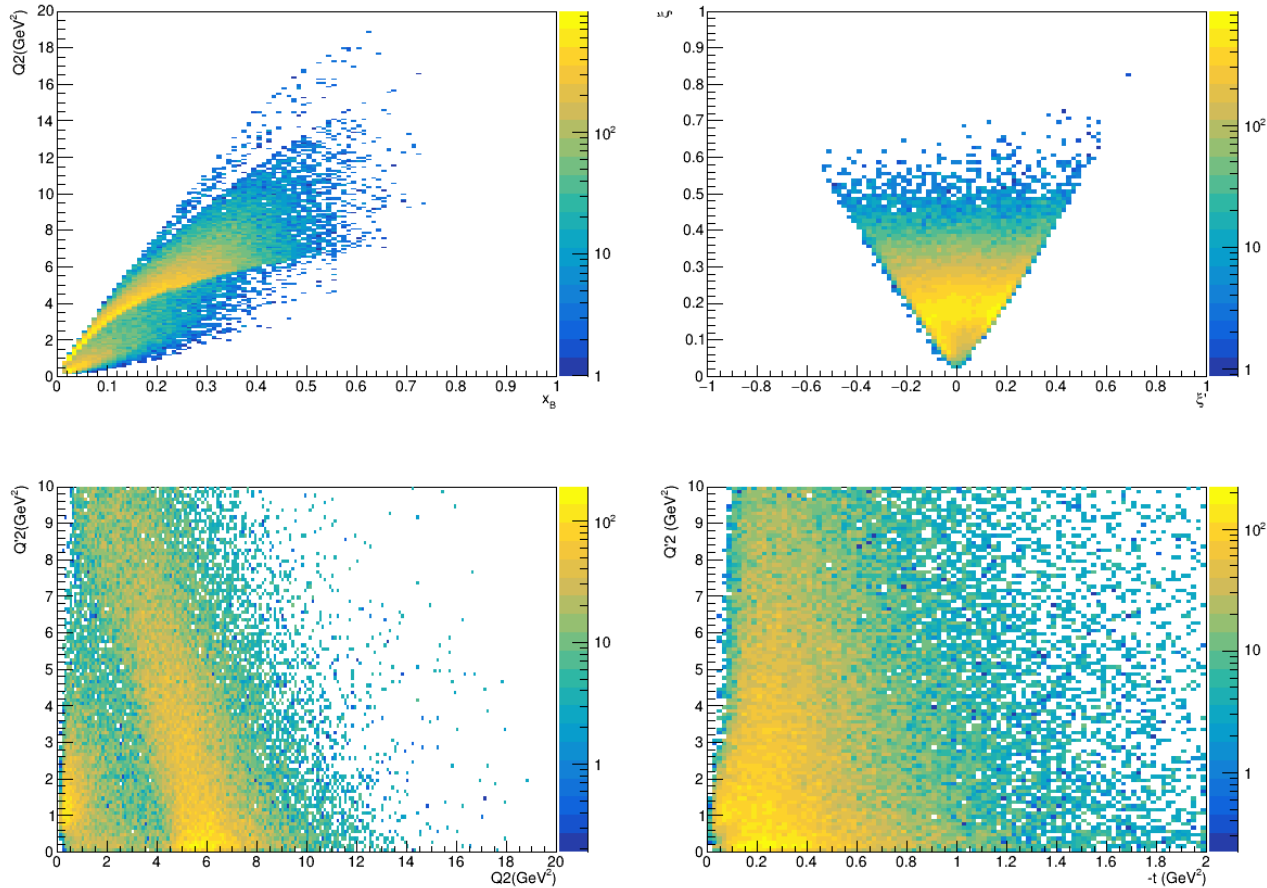
Kinematical coverage 11 GeV



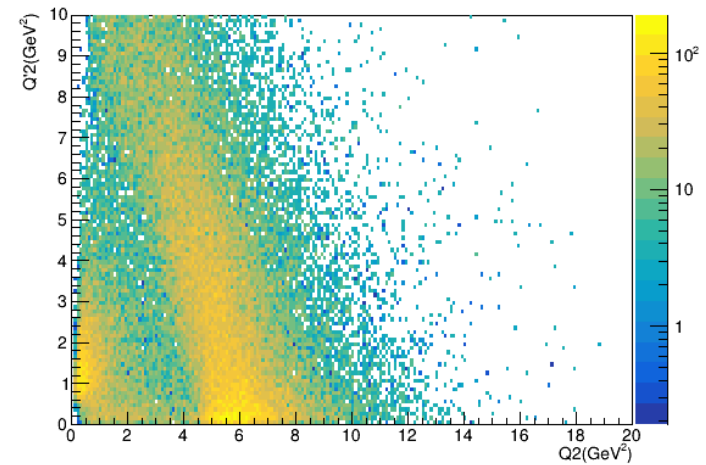
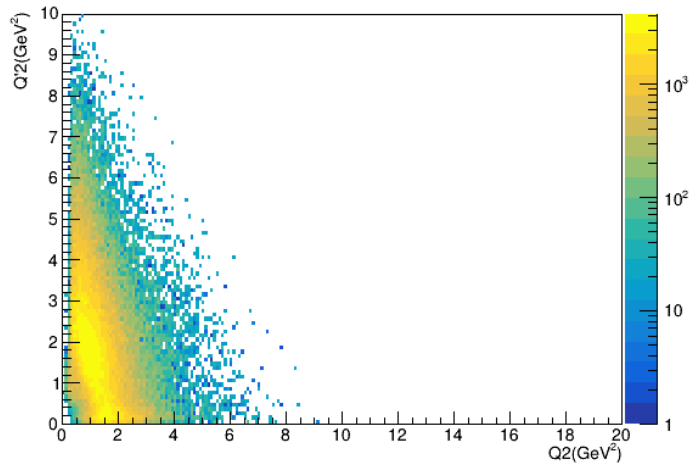
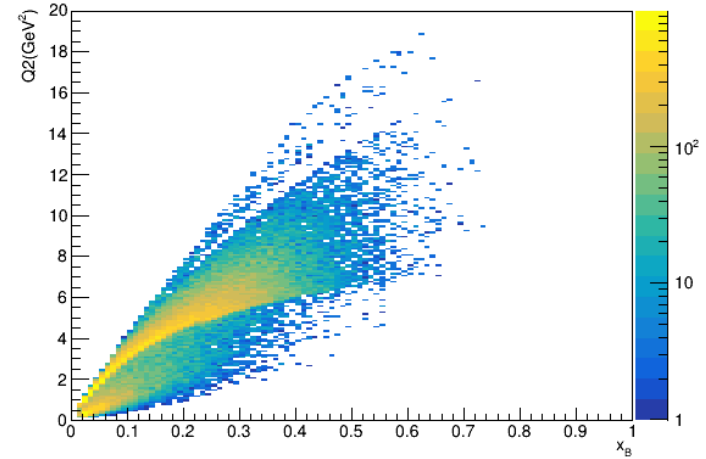
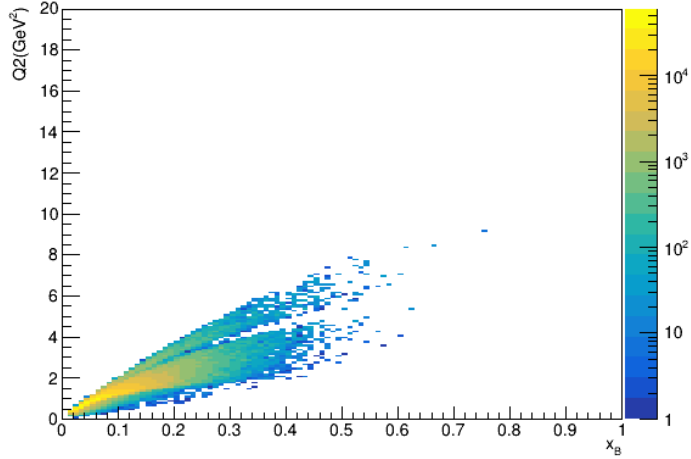
Kinematical coverage 22 GeV

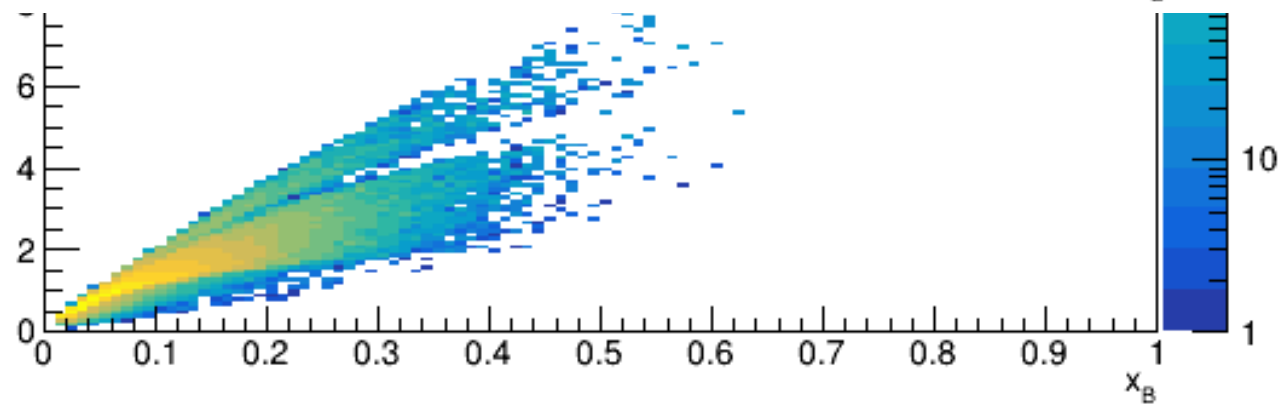
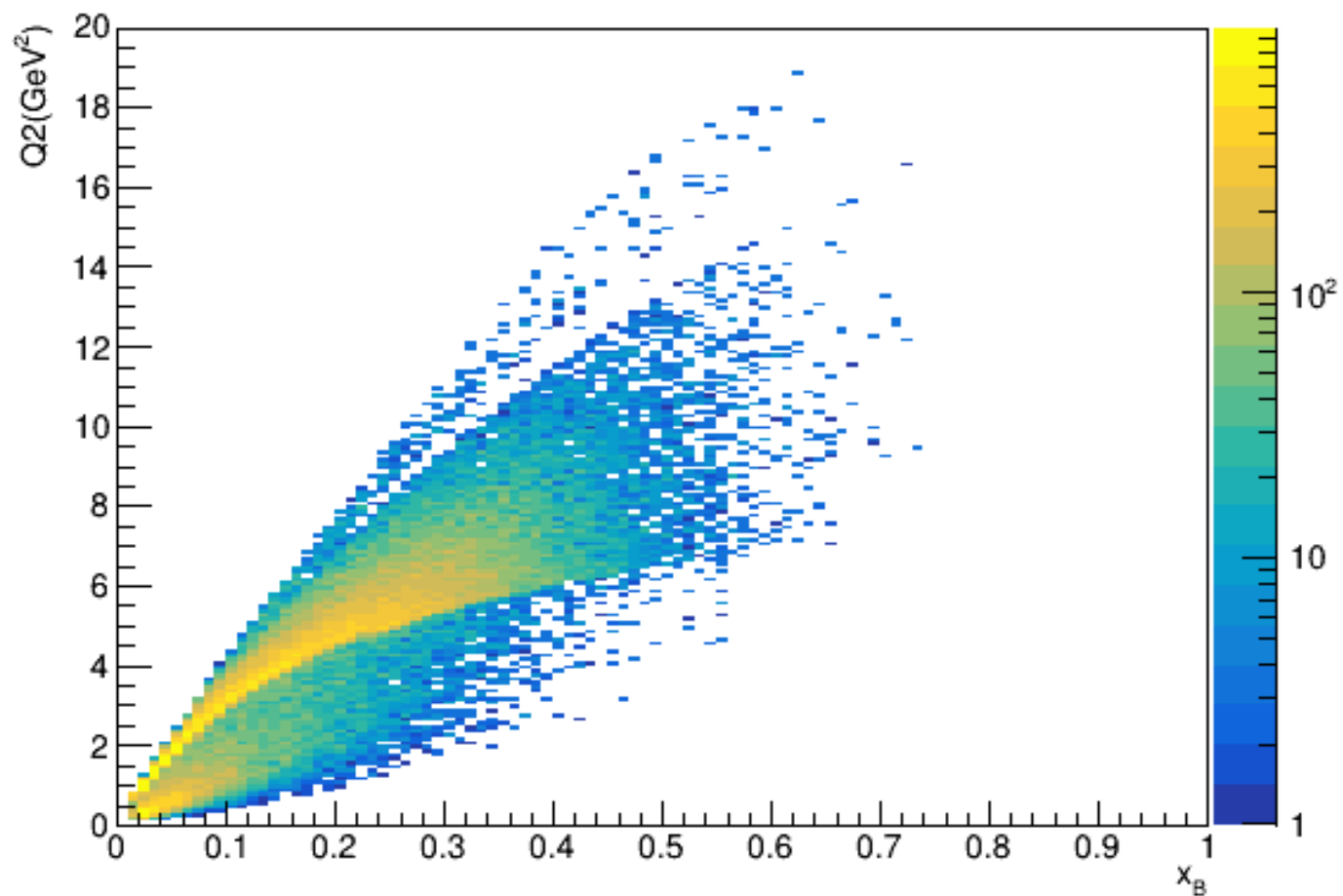


Kinematical coverage 22 GeV

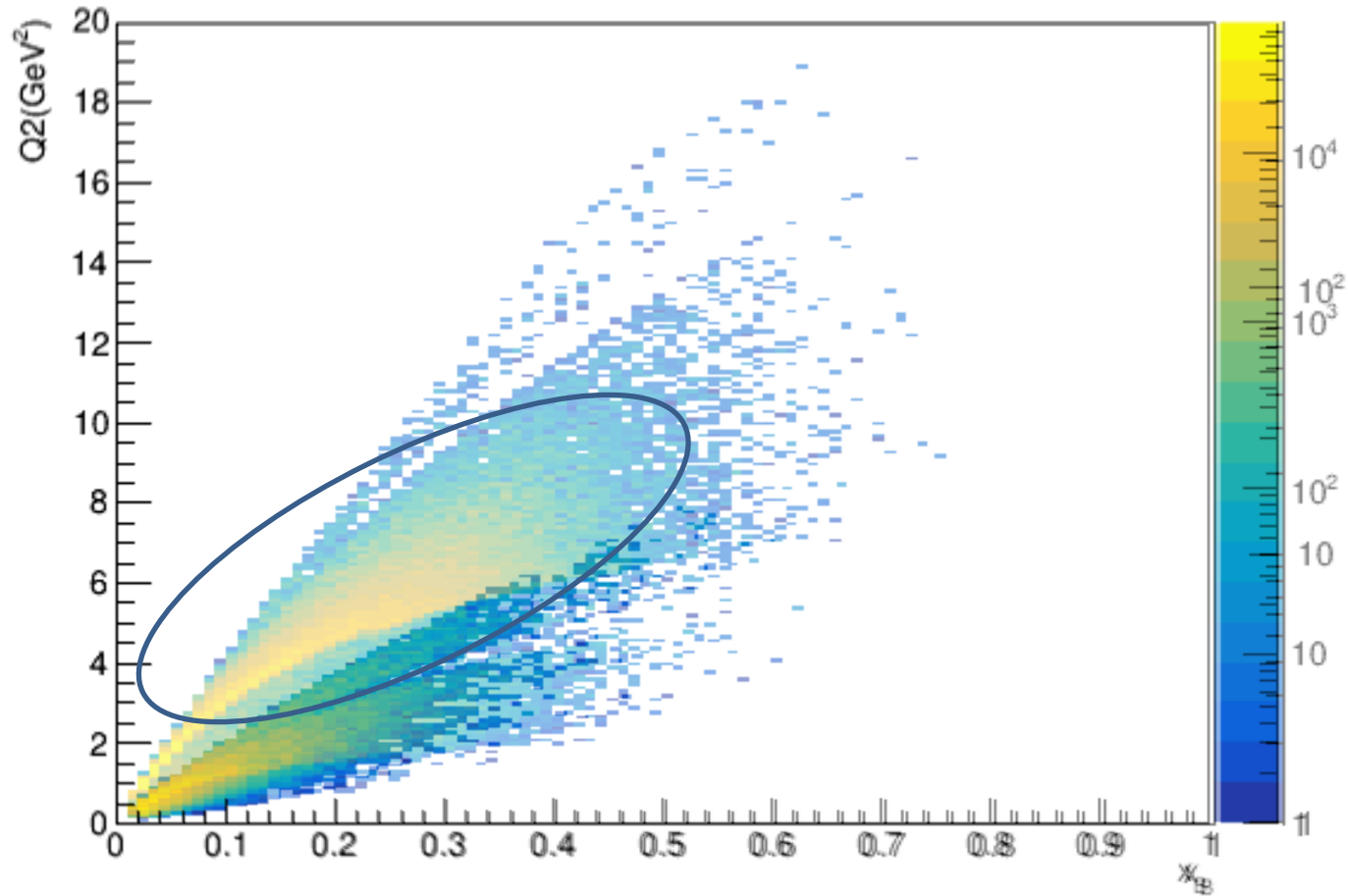


11 GeV vs 22 GeV

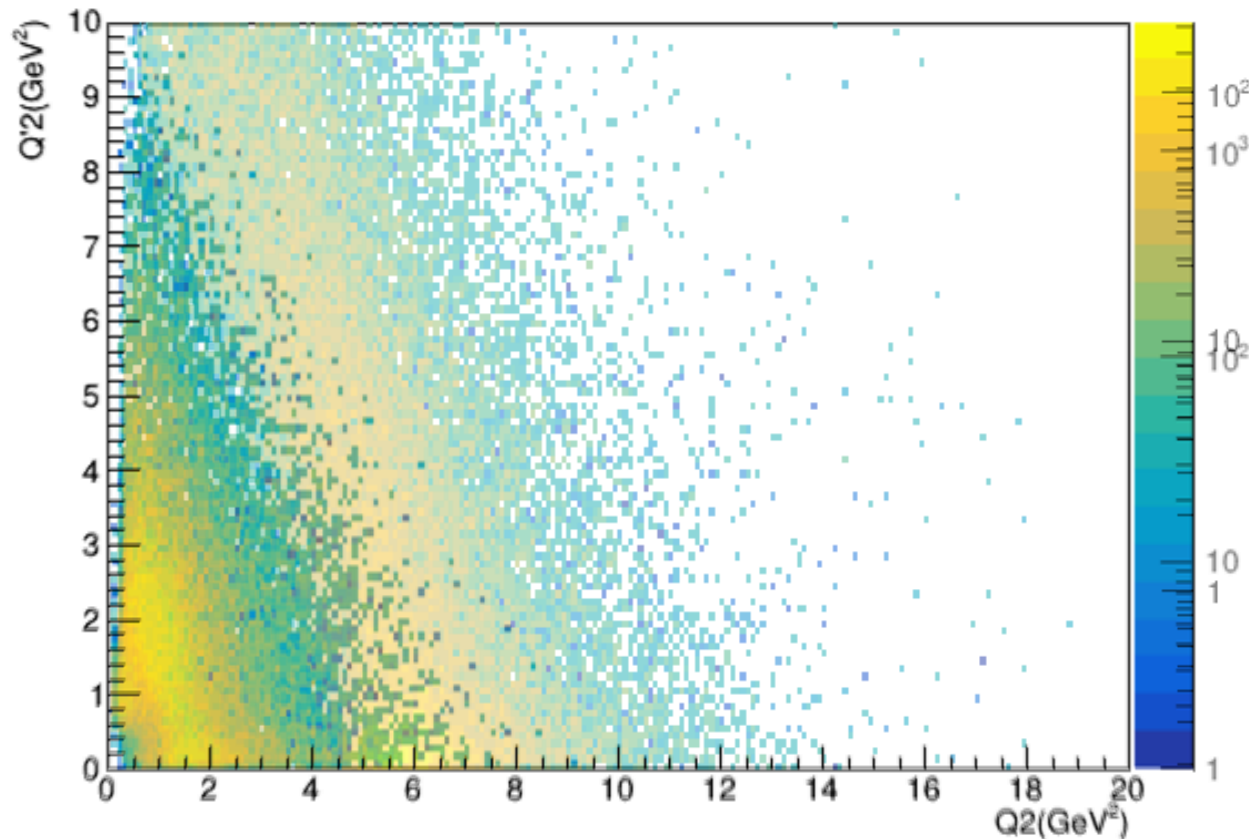




11 GeV vs 22 GeV



11 GeV vs 22 GeV



Much better Q^2 Q'^2
coverage

Want Q^2 and Q'^2 large
enough for
factorization